SECTION I
RESEARCH IN PROGRESS

NUCLEAR REACTIONS
(EXPERIMENTAL)

ENERGY DEPENDENCE OF LIGHT PARTICLE PRODUCTION

Z.M. Koenig, G.D. Westfall, L.H. Harwood,
B.V. Jacak, S. Angius, D. Ardouin, G.M. Crawley,
M.V. Curtin, C.K. Gelbke, B. Hasselquist,
W.G. Lynch, D. Morrissey, A.D. Panagiotou,
D.K. Scott, and M.B. Tsang

The behavior of nuclear matter in high energy nucleus-nucleus collisions has been described by several different models, which include thermal[1], intranuclear cascade[2], hydrodynamics[3], coalescense[4], direct knockout[5], and combinations of these ideas. Different characteristics of the emission of light particles can be described by these models. This study is concerned particularly with incident beam energies between 20 to 40 MeV/nucleon. A quantum statistical model of Schulz, et al[6]. predicts that the ratios of the production cross sections of composite particles to protons will have a minimum predicted to occur at a critical temperature of approximately 20 MeV corresponding to a beam energy of 40 MeV/nucleon for asymmetric systems.

On September 13, 1982 the first experiment was performed with the K500 Superconducting Cyclotron using a 35 MeV/nucleon ^{12}C (charge state +4) beam with an average current of about 3 particle nanoamps. A natural self-supporting gold foil of 9.6 mg/cm^2 target was used. Subsequently beams of ^{12}C and alphas were used on carbon and gold targets at 20,25,30 and 40 MeV/nucleon. The angular distributions and energy spectra for light particle production were measured with two detector telescopes each made up of a 400 micrometer thick Si delta-E counter and a 10 cm thick NaI E-counter. The data were recorded event by event through CAMAC using a PDP 11/23 coupled to a VAX 11/750 and were analyzed off-line using the VAX. The spectra were normalized using a shielded Faraday cup coupled to a BIC charge integrator. The overall normalization was reproducible to within 5%. The analysis of the 20,25,30 and 40 MeV/nucleon data is now in progress.

In Fig. 1 the double differential cross sections for 35 MeV/nucleon ^{12}C + Au leading to p,d,t,^{3}He,^{4}He, and ^{6}He are shown for the laboratory angles 40,60,75,90,105,120, and 140 degrees. The errors depicted are statistical. The proton spectra span an energy range of 10 to 150 MeV. The solid lines correspond to single moving source fits as in Ref. 6 in which a relativistic Boltzmann distribution was assumed in the rest frame of the moving source. In Figs. 2 and 3 the extracted parameters for 35 MeV/nucleon ^{12}C+Au are compared with the systematics of ^{16}O and ^{20}Ne induced reactions on heavy targets.

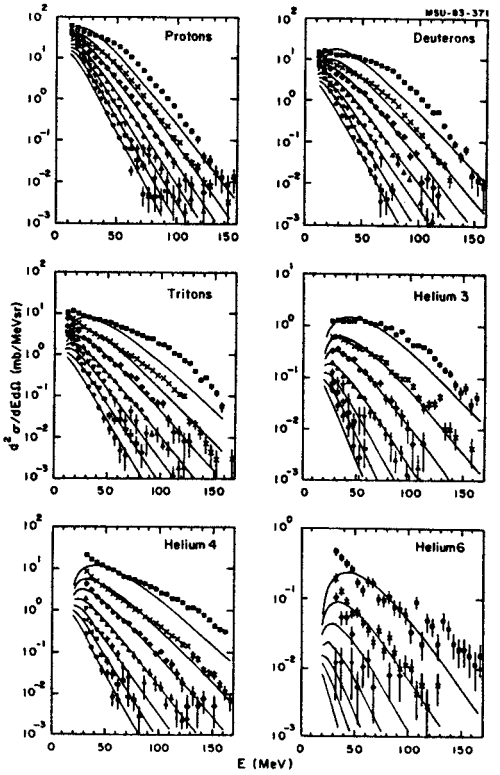

Fig. 1. Energy spectra for 35 MeV/nucleon ^{12}C+Au leading to p, d,t, ^{3}He and ^{4}He. The angles measured are 40,60,75,90, 105, 120, and 140 degrees in the laboratory. The errors depicted are statistical. The solid lines correspond to moving source fits as described in the text.

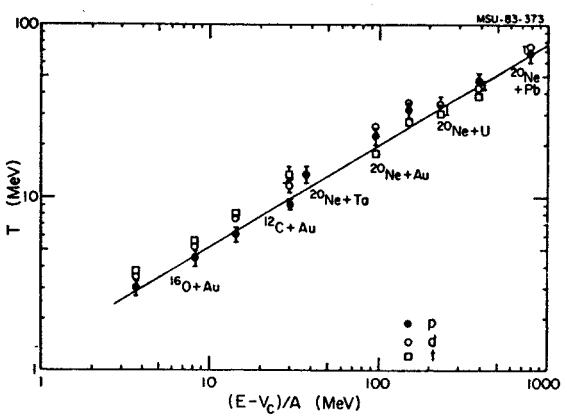

Fig. 2. Temperatures for p,d, and t extracted using a moving source parametrization as in the text compared with corresponding values for ^{16}O and ^{20}Ne induced reactions[8] plotted as a function of laboratory energy per nucleon above the coulomb barrier. The solid line is a line to guide the eye.

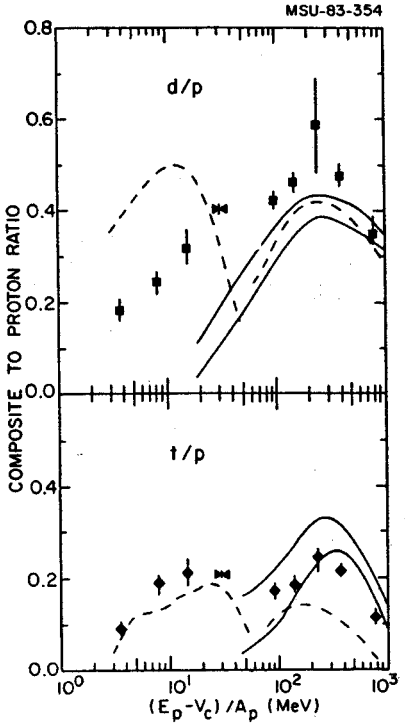

Fig. 3. Extracted composite to proton ratios using a moving source parameterization as in the text compared with systematics of ^{16}O and ^{20}Ne induced reactions on heavy targets[8] plotted versus laboratory energy per nucleon above the coulomb barrier. ■ And ◆ refer to ^{16}O and ^{20}Ne induced reaction while the ⋈ symbols refer to the present work. The solid lines correspond to a hydrodynamic calculation incorporating chemical equilibrium[7] at freeze-out densities of 0.1 and 0.7 times normal nuclear density and the dashed lines correspond to a quantum statistical calculation[6].

Fig.3 shows the experimental composite to proton ratio data as compared to the quantum statistical calculation[6] (dashed line) and a hydrodynamic calculation with chemical equilibrium[7] (solid line). The quantum statistical model shows the characteristics of a critical temperature in which there is a dip in the composite to proton ratios. At temperatures above this critical temperature, the quantum statistical model takes on a thermal-chemical equilibrium character which is in agreement with the hydrodynamic calculation incorporating chemical equililbrium. Whereas below the critical temperature, the quantum statistical model describes the system as a coexistence of liquid-vapor phases, indicating a first order phase transition near the critical temperature. The present data show no direct evidence of this phase transition for the deuteron to proton ratio, yet the triton to proton ratio seems to follow the trend of the quantum statistical model, indicating possible evidence for a phase transition.

1. J.I. Kapusta, J. Gosset, and G.D. Westfall, Phys. Rev. C18, 844(1978).
2. Y. Yariv and Z. Fraenkel, Phys. Rev. C24, 488(1982).
3. H. Stocker, C. Riedel, Y. Yariv, L.P. Csernai, G. Buchwald, G. Graebner, J.A. Maruhn, W. Greiner, K. Frankel, M. Gyulassy, B. Schurmann, G.D. Westfall, J.D. Stevenson, J.R. Nix, and D. Strottman, Phys. Rev. Lett. 47, 1807(1981).
4. H.H. Gutbrod, A. Sandoval, P.J. Johansen, A.M. Poskanzer, J. Gosset, W.G. Meyer, G.D. Westfall, and R. Stock, Phys. Rev. Lett. 37, 667(1976).
5. R.L. Hatch and S.E. Koonin, Phys. Lett. 81B, 1(1979).
6. H. Schulz, L. Munchow, G. Ropke, and M. Schmidt, Phys. Lett. 119B, 12(1982).
7. H. Stocker, G. Buchwald, G. Graebner, P. Subramanian, J.A. Maruhn, W. Greiner, B.V. Jacak, and G.D. Westfall, Nucl. Phys. A400, 63c(1983).
8. G.D. Westfall, B.V. Jacak, N. Anantaraman, M.V. Curtin, G.M. Crawley, C.K. Gelbke, B. Hasselquist, W.G. Lynch, D.K. Scott, B.M. Tsang, M.J. Murphy, T.J.M. Symons, R. Legrain, and T.J. Majors, Phys. Lett. 116B, 118(1982).

PREEQUILIBRIUM EMISSION OF INTERMEDIATE MASS FRAGMENTS IN THE 197AU + 12C REACTION AT 30 MeV/A

H. Utsunomiya, D.J. Fields, C.B. Chitwood,
C.K. Gelbke, W.L. Lynch, A.D. Panagiotou
and M.B. Tsang

There have been some experimental evidences[1,2] that in heavy-ion reactions intermediate mass fragments between 4He and fission fragments are emitted with kinetic energies considerably lower than that corresponding to the quasi-elastic (fragmentation) process. Their kinetic energies show narrow distributions around the exit channel Coulomb barrier expected in a binary reaction, suggesting the complete relaxed components of the incident kinetic energy. The observation appears consistent with recent theoretical predictions[3,4,5] that disintegration of the highly excited (compound) nucleus takes place via emission of the intermediate mass fragments besides the usual decay modes such as evaporation of light particles (n,p, α etc.) and fission. On the other hand, non-equilibrium feature of the intermediate mass fragment emission has been seen in their forward-peaked angular distributions as well as the charge(mass) distributions[1].

In this note, we report on preequilibrium emission of the intermediate mass fragments observed in the bombardment of ^{197}Au with 30 MeV/u ^{12}C projectiles. Our attention is particularly paid to detailed energy distributions of the fragments. This work shows that the preequilibrium spectra are characterized by the Maxwell-Boltzmann distribution with significantly slow exponential slopes and low barrier heights, suggesting a strong nuclear distortion and high nuclear temperatures of the associated system.

The experiment was performed at the National Superconducting Cyclotron Laboratory of Michigan State University using a 30 MeV/u ^{12}C beam. A self-supporting ^{197}Au metallic foil of 580μm thickness was used as a target. Energy spectra of the intermediate mass fragments were measured at 30°,50°,70° and 120° using a ΔE-E1-E2 telescope comprized of a Frish-grid ionization chamber[6] and two 430 μm silicon surface barrier detectors. The angular range was chosen to be backward enough from the Coulomb trajectory of the grazing collision to eliminate contributions from the peripheral reactions such as transfer and projectile fragmentation. The ionization chamber was operated with pressure of 80 torr of an argon (90%) - methan(10%) mixture. The energy calibration for the Si counter was done by means of the chopper-pulser system[7] and checked with an α-source of ^{244}Cm and elastic scattering of 15 MeV/u-^{12}C off the gold target. The calibration for the ionization chamber was made by deducing energies ΔE deposited by various elements from a two dimentional ΔE-E map using the effective thickness of the ionization chamber. The effective thickness was calculated for 100% argon of 80 torr at 273°K. The overall error involved in the absolute total kinetic energies including energy losses within the target was estimated to be ±3 MeV. The uncertainty in the absolute cross section was estimated to be less than 20%.

The measured cross sections and energy spectra were transformed into those in the c.m. system assuming a binary reaction, i.e., ^{197}Au + ^{12}C → the intermediate mass fragment + the residual nucleus, where the mass number of the fragment was taken to be twice the atomic number.

The angular distributions in the c.m. system are shown in Fig.1 for various elements, which are similar to those reported in Ref.1. It is remarkable that the angular distributions of the intermediate mass fragments with z ≤10 are

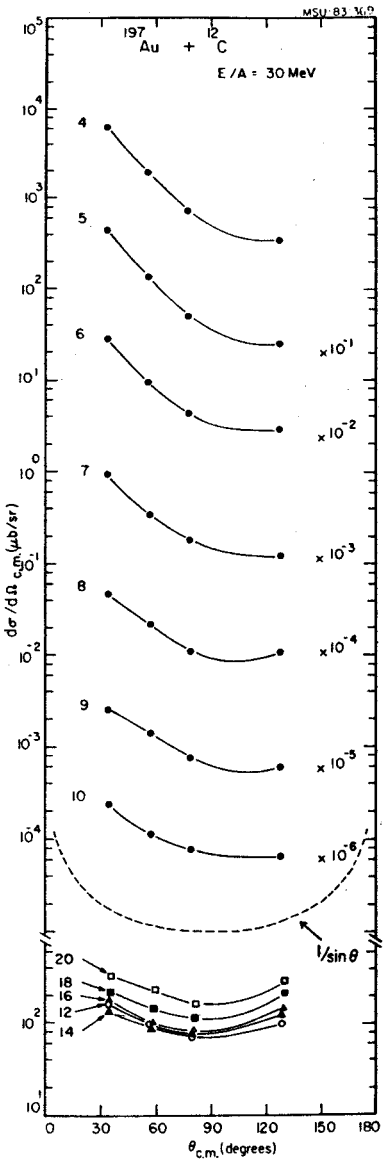

Fig. 1. Center-of-mass angular distributions of various intermediate mass fragments measured in the ^{197}Au + ^{12}C reaction at 30 MeV/u. The solid curves are to guide the eye.

strongly forward-peaked and the forward peaking gradually decreases with the increase of Z. Since the present angular range is relatively backward, the above fact appears to indicate that the fragments are emitted at an intermediate stage going on the way to the formation of the compound nucleus.

We observed a large amount of fission cross section which contributes to cross sections of elements down to z ≈11. In fact, the angular distributions of these elements are symmetric about 90° and exhibit a shape nearly close to 1/sin θ, which is characteristic of decay of a rotating system with a large angular momentum.

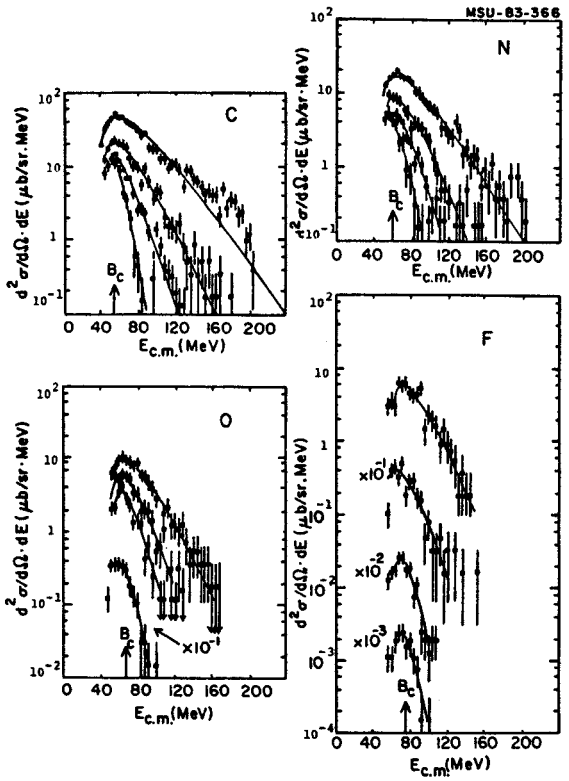

Fig. 2. Center-of-mass energy spectra of various intermediate mass fragments measured at 30°, 50°, 70° and 120° in the ^{197}Au + ^{12}C reaction at 30 MeV/u. The solid curves are the best fits by the evaporation formula explained in the text. A small bump around 180 MeV seen in the carbon spectrum at 30° is the folding back component which punched through the detector telescope.

Fig.2 shows the c.m. energy spectra of several elements. The location of rapid fall off in the low energy side is nearly independent of emission angles. This seems to indicate that when the fragments are emitted, they have to ride across the Coulomb barrier between the fragment and the residual nucleus in the c.m. system. In other word, the fact lends a strong suppor to the present assumption of a binary reaction. However, it should be noted that the barrier heights are significantly smaller than expected in the spherical configuration of the two touching nuclei. The arrows denoted by B_c in Fig. 2 indicate locations of the spherical Coulomb barriers calculated using the radius parameter given in Ref.1, i.e., $R=1.225(A_1^{1/3} + A_2^{1/3}) + 2$ fm. The significantly low barrier heights seem attributed to a strong nuclear distortion of the associated system as was pointed out by Knox, Quinton and Anderson[8] for the case of evaporation of light particles from highly excited compond nucleus.

The energy spectra of z≤10 measured at 120° exhibit shapes of evaporation spectra with almost same exponential slopes, which is consistent with the fully thermarized components of the incident kinetic energy. It is remarkable that the forward spectra are very broad but still have the Maxwell-Boltzmann distributions with gentle exponential slopes, suggesting high nuclear temperatures of the relevent system.

The statistical evaporation formula[9].

$$N(E_i^{cm}) \propto E_i^{cm}\, \sigma_{inv}(E_i^{cm}) \exp(-E_i^{cm}/T_i) \qquad (1)$$

was employed in order to parameterize the non-equilibrium spectra of the intermediate mass fragments by the "barrier height" B_i and "spectral temperature" T_i of the associated system. Here, E_i^{cm} is c.m. kinetic energy of element i and σ_{inv} the inverse cross section which we take, for simplicity, to be $\sigma_{inv}(E_i^{cm}) = \pi R_i^2 (1 - B_i/E_i^{cm})$. Equation (1) implicitly assumes the cold fragment emission and spin-independent temperature. It seems that the former assumption is not necessarily reasonable in the case of the intermediate mass fragment emission. In that case, the secondary decay of the excited fragments modifies the final mass (charge) distributions to some extent. However, it is shown that the two assumptions do not introduce a serious change to the nuclear temperatures when we consider the statistical emission of the fragments from the compound nucleus. Consider the emission of the composite fragment with excitation energy ε corresponding to the temperature T. The resultant temperature $T_{j,\varepsilon}$ can be estimated in a manner similar to that taken in Ref. 10 by $T_{j,\varepsilon}/T = [1 - (E_{rot}(j) + \varepsilon)/U_{av}]^{1/2}$, where $E_{rot}(j)$ is rotational energy and U_{av} average excitation energy of the residual nucleus. ε is related to T with $\varepsilon = aT^2$ and the level density parameter a is connected to the fragment mass F with $a = F/16$. Using values of the critical angular momentum for complete fusion (60ħ) [11] and the rigid body moment of inertia, the deviation of $T_{j,\varepsilon}$ from T was found to be 5-10%.

The energy spectra of the intermediate mass fragments were well reproduced by the evaporation formula as shown by solid curves in Fig.2. The

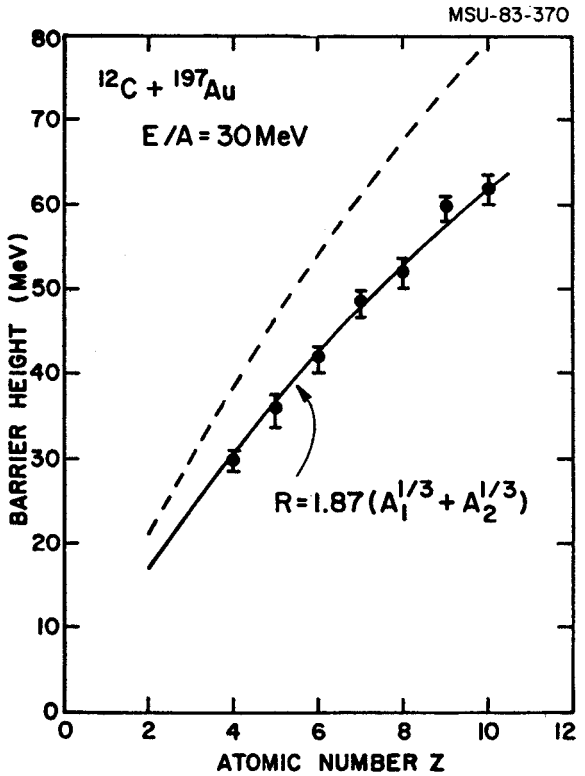

Fig. 3. Values of the barrier heights deduced for various elements. The dashed curve shows the Coulomb barrier heights at the spherical configuration of two touching nuclei calculated using $R=1.225(A_1^{1/3}+A_2^{1/3})+2$ fm[1]. The solid curve shows the best fit of the experimental barrier heights by using the effective Coulomb radius parameter r_{eff} =1.87 fm in $R=r_{eff}(A_1^{1/3}+A_2^{1/3})$.

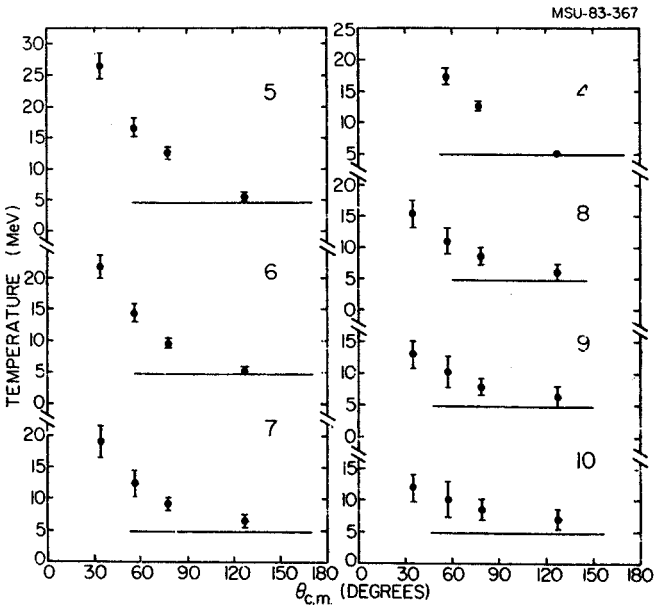

Fig. 4. Values of the "spectral temperatures" deduced for various elements. The solid lines show the equilibrium temperature in each case.

best-fit values of B were constant within 5 MeV, being independent of emission angles. The values of B averaged over emission angles are shown in Fig.3 as a function of the atomic number of the element. The Coulomb barrier heights[1] of two touching spherical nuclei in the exit channel are shown by the dashed curve in Fig.3. It should be noted that the experimental barrier heights are lowered by 8-20 MeV from the exit channel Coulomb barrier at the spherical configuration. It is instructive to estimate the magnitude of the strong nuclear distortion using the effective Coulomb radius parameter r_{eff} in $R=r_{eff}(A_1^{1/3}+A_2^{1/3})$. The best fit was obtained with r_{eff}=1.87 fm, which is shown by the solid curve in Fig.3.

Fig.4 shows the best-fit values of T as a function of emission angles θ. In all cases, the spectral temperatures decrease monotonically with increasing angles and nearly reach, at 120°, the equilibrium temperature T_{eq} calculated from $T=(U_{av}/a)$ and a=A/16 with the mass number A of the residual nucleus.

Now let me (H.U.) interprete the spectral temperatures based on the hot spot model[12] I assume that the source of the intermediate mass fragments is a locally equilibriated system (hot spot) sitting on the surface region of the composite system comprized of projectile and target. Strong radial and tangential frictional forces in the entrance channel are supposed to be responsible for the formation of the hot spot and the strong nuclear distortion mentioned above. Such interpretation was made by Nomura et al.[13] in low energy (°≤10 MeV/u) heavy-ion reactions, where emission mechanism of fast light particles was described in terms of tangential emission from a single hot spot. For the intermediate mass fragments, the origin might be an ensemble of multi-sources (hot spots) that are formed with different impact parameters and proceed to the decay processes in their own ways. Moreover, not only cold but also excited fragment, therefore, its sequential decay in flight should be presumably taken into account. It should be pointed out that if the spectral temperature higher than 20 MeV, deduced for Z=5,6 at 50°, is achievable in the present reaction, it must be associated with much smaller internal degrees of freedom than given by the level density parameter for uniform Fermi gas, i.e., a=A/16. Quantitative consideration of the spectral temperatures seems subject to a future study because of a lack of detailed knowledge of the "local" degrees of freedom, which might be addressed by incorporating non-equilibrium aspect in the local heating or dynamical aspect of collision.

Fig.5 shows the spectral temperatures minus T_{eq} as a function of θ. It should be noted that the quantity $T-T_{eq}$ falls almost exponentially with increasing θ, i.e., $T-T_{eq} \propto e^{-\theta/\theta_0}$ and the decay constant θ_0 is nearly the same for all elemants. Despite of a lack of full understanding of the "kinematics" in the hot spot model, it is informative to estimate the internal decay time

τ_{hs} of the hot spot following the prescription of Ref. 14. The decay constant σ was converted into τ_{hs} from a relation of $\sigma=\omega.\tau_{hs}$ on the assumption that the emission angle is connected with the

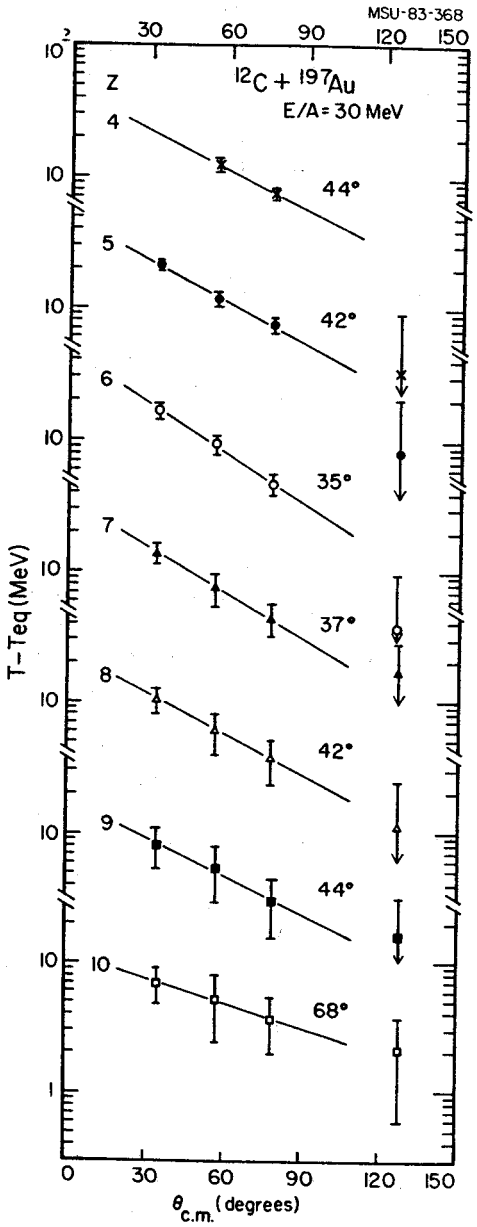

Fig. 5. $T-T_{eq}$ versus emission angles. The straight lines show the least-squares fits for the data at forward angles. The decay constants σ derived from the straight lines are shown in the figure.

rotational time of the composite system in a unique way. The angular velocity ω of the rotatinal motion was calculated at the sticking condition[15] using the rigid body moment of inertia. The results are listed in Table 1. Because of the strong nuclear distortion the rigid body moment of inertia with r_{eff} =1.87 fm was used. Assuming that the entrance angular momenta responsible for the present reaction lie between the maximum angular momentum (147 $\hbar$) and the critical angular momentum (60 $\hbar$) for complete fusion[11], we conclude that τ_{hs} rangs from 0.79 to 3.7 x 10^{-21} sec, being comparable to preequilibrium emission time of α particles determined in the literatures[16].

1. L.G. Moretto et al., Phys. Lett. 58B, 31(1975); L.G. Moretto et al., Nucl. Phys. A255, 491(1975).
2. C.B. Chitwood et al., Phys. Lett. 131B 289 (1983).
3. L.G. Moretto, Nucl. Phys. A247, 211(1975).
4. D.H.E. Gross et al., Z. Phys. A309, 41(1982).
5. W.A. Friedman and W.G. Lynch, Phys. Rev. C28, 16(1983)
6. J. Barrette et al., Nucl. Instr. and Meth. 126, 181(1975).
7. F.S. Goulding et al., IEEE, Trans. Nucl. Sci. 13, 514(1966).
8. W.J. Knox, A.R. Quinton and C.E. Anderson, Phys. Rev. 120, 2120(1960).
9. J.M. Blatt and V.F. Weisskopf, Theoretical nuclear physics (Wiley, New York, 1952); T. Ericson, Adv, in Phys. 9, 425(1960).
10. D.C. Williams and T.D. Thomas, Nucl. Phys. 53, 577(1964).
11. W.W. Wilcke et al., Atomic data and nuclear data tables 25, 389(1980).
12. R. Weiner and M. Westrom, Nucl. Phys. A286, 282(1977).
13. T. Nomura et al., Phys. Rev. Lett. 40,694(1978); H. Utsunomiya et al., Nucl.Phys. A334,127(1980).
14. T. Nomura et al., J. Phys. Soc. Japan 46, 335(1979).
15. W.U. Schroder and J.R. Huizenga; Annu. Rev. Nucl. Sci. 27, 465(1977).
16. H. Ho et al., Z. Phys. A283,235(1977).

TABLE 1 Internal decay time of the hot spot estimated in the 197Au + 12C reaction at 30 MeV/u.

z	σ (deg)	τ_{hs}[1] (10^{-21} sec)	τ_{hs}[2] (10^{-21} sec)
4	44	0.99	2.4
5	42	0.94	2.3
6	35	0.79	1.9
7	37	0.83	2.0
8	42	0.94	2.3
9	44	0.99	2.4
10	68	1.5	3.7

1) Deduced for the maximum angular momentum (147 $\hbar$)[11]. The angular velocity ω calculated at the sticking condition[15] is 7.8 rad/10^{-20}sec.

2) Deduced for the critical angular momentum (60 $\hbar$) for complete fusion[11]. The angular velocity ω calculated at the sticking condition[15] is 3.2 rad/10^{-20}sec.

SEARCH FOR MULTIPARTICLE JETS

B.E. Hasselquist, G.D. Westfall, L.H. Harwood,
R.S. Tickle*, B.V. Jacak, Z.M. Koenig,
G.M. Crawley, T.J.M. Symons**, J.P. Dufour**

In the study of nucleus-nucleus collisions at intermediate energies one can conceive of a number of possible measurements which may lead to a better understanding of the dominant processes. Within the scope of the two experiments to be described in this report are four such measurements.

In the first measurement we detect a projectile-like fragment at small angles and at velocities near the beam velocity in coincidence with light charged particles near 90° on the opposite side of the beam. The light particles are detected in a 7 element multidetector array called the Hit Detector In the second measurement we study an analogous case as we detect a slow target-like fragment near 90° in coincidence with light charged particles at forward angles on the opposite side of the beam, again in the Hit Detector.

Experimental data of Meyer et. al.[1], present evidence for 180° azimuthal correlations between fast, sidewards emitted light fragments and slow, heavy fragments in fast nuclear collisions. The nuclear fluid dynamical model has been used to interpret this large collective momentum transfer in collisions of intermediate impact parameter. Because of the large pressure of the hot, dense matter at 2 to 3 times normal nuclear density in the impact region and its subsequent expansion, the projectile and target residues are pushed apart from each other in the scattering plane. A hydrodynamical description of nuclear collisions [2] at intermediate energies predicts that for non-central collisions we have an effect which has been viewed as a highly inelastic bounce-off of the projectile from the target. In this process, the projectile is scattered by a compression potential to the side, as is the strongly hit target matter, while a rather large part of the target stays bound. The projectile-like fragment having a high excitation energy will explode into a large number of small, higher energy particles. Thus, this process can be detected experimentally by measuring a large target fragment with rather large perpendicular momentum in coincidence with the small fragments going into the forward hemisphere, correlated to the target fragment at 180° in the azimuthal angle.

In a third measurement we detect a light charged particle and then look for coincident light charged particles on the opposite side of the beam in the Hit Detector. This measurement is important for determining to what extent colliding nuclei interact solely as collections of nucleons.

One limit of the nuclear cascade model is the single scattering model in which it is assumed that the primary contribution to the light particle spectra comes from single nucleon-nucleon scattering[4,5]. In the other limit are the thermal models which assume some degree of equilibration of the target and projectile nucleons followed by statistical emission of light particles. One should be able to differentiate between these two limits by detecting a light particle at some intermediate angle and simultaneously measuring the light particle distribution on the opposite side of the beam. In our experiment the detector angles were chosen so that the angles where a free nucleon would be scattered were bracketed. Also, the large angular acceptance of the Hit Detector allows the measurement of the coincident particle even though the kinematical region where it should be observed is large because of the fermi momenta of the two nuclei.

It is quite conceivable that there exist other exotic collective phenomena which could leave as their signature large multiplicities of light charged particles. For example, the onset of the disintegration or explosion of the localized hot region in a nuclear collision is predicted to occur in the energy region of 20-100 Mev/nucleon. A high multiplicity of nucleons should be emitted in such an explosion with a corresponding lack of composite particles. Another possibility is the concept of Fermi jets, which is characteristic of the mean field or long mean free path approximation. The fourth measurement in this experiment is then an attempt to identify events with a high multiplicity of light particles. This was done by triggering the Hit Detector on itself.

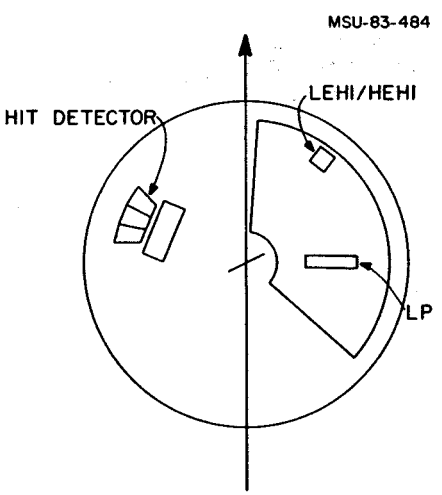

Fig. 1. Experimental setup in the LEBL 60" chamber during the Bevalac run.

The first experiment was performed March 11, 1983 at the Bevalac at LBL using a ^{40}Ar beam at 100 Mev/A and a Au target. The experimental setup

is shown in figure 1. The Hit Detector[3] consisted of seven E-ΔE plastic scintillator-CaF_2 phoswich telescopes mounted in an array behind a 3 plane multiwire proportional counter (MWPC). The array covered a total of approximately 100 msr for a given angle setting. The E and ΔE signals were obtained by gating charge integrating ADC's with a prompt 80 nsec wide gate for the E signal and a 1 μsec wide gate delayed by 240 nsec for the ΔE signal. Energy, particle identification, and angular information were derived for p,d,t, and ^3He, ^4He for 20 Mev/A < E < 150 Mev/A and 40° ≤ θ ≤ 100°. A scatter plot for a representative plastic scintillator telescope is shown in figure 2. The Hit Detector was gated in coincidence with the three trigger detectors on the opposite side of the beam which consisted of two silicon detector telescopes, a three element one for low energy heavy ions (LEHI) and a five element one for high energy heavy ions (HEHI) both measuring particles with Z > 2 and a Si-NaI light particle telescope (LP) measuring p,d,t and 3He,4He. The positions of the trigger detectors are given in Table 1. The Hit Detector was also allowed to trigger on itself. Singles data was taken for normalization purposes.

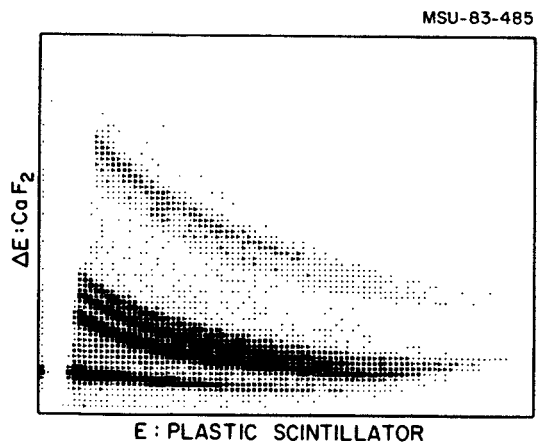

Fig. 2. Delta E vs. E scatter plot for a typical plastic scintillator-CaF_2 telescope in the Bevalac run.

Table 1. Detector angles for the Bevalac run.

Bevalac Run	100 Mev/A ^{40}Ar + Au	
Detector	Theta (Deg)	Phi (Deg)
HEHI	30	+10
LEHI	30	-10
LP	90	0
HIT DET	40-100	0,+/-6

The second experiment was performed Apri. 25, 1983 at NSCL as part of the first scheduling period of the K500 using a ^{12}C beam at 30 Mev/A and Au and Al targets. The experimental setup is shown in figure 3 and is similar to the Bevalac setup with the addition of the ion chamber (IC) at 90 for detection of slow target-like fragments. The trigger detector positions are given in Table 2.

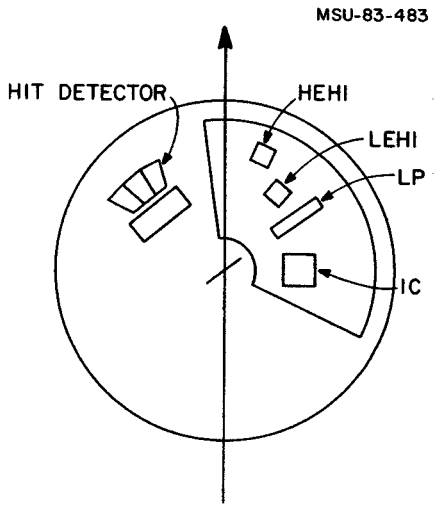

Fig. 3. Experimental setup in the NSCL 60" chamber during the MSU run.

Table 2. Detector angles for the NSCL run.

NSCL Run	30 Mev/A ^{12}C + Au,Al	
Detector	Theta (Deg)	Phi (Deg)
HEHI	15	0
LEHI	25	0
LP	45	0
IC	90	0
HIT DET	40-100	0,6.5,13

The MWPC functioned properly during the Bevalac run only for the calibration runs, after which time it developed a high voltage arcing problem. The operation of the array of plastic scintillators was not affected by this problem, however.

At the present time the analysis of the Bevalac data is proceeding in its preliminary stages with the analysis of the NSCL data to be done upon completion of the preliminary Bevalac data analysis.

* University of Michigan
** Lawrence Berkeley Laboratory

1. W.G. Meyer,H.H. Gutbrod, CH. Lukner, and A. Sandoval, Phys. Rev. C22. 179 (1980).
2. H. Stocker, J.A. Maruhn, and W. Greiner, Z. Physik A293, 173-179 (1979) and Phys. Rev. Lett. 44. 725 (1980)
3. B.E. Hasselquist, G.M. Crawley, R.S. Tickle, L. Richarson, G.D. Westfall, MSU Cyclotron Lab Annual Report 78,79 (1981-1982) and B. Tickle, B. Hasselquist, G. Crawley, B. Tsang and J. Yurkon MSU Cyclotron Lab Annual Report 77 (1981-1982)
4. B. Jakobsson, et. al. Phys. Lett. 102B, 121(1981)
5. R.L. Hatch and S.E. Koonin, Phys. Lett. 81B, 1(1979)

PRODUCTION OF MIDRAPIDITY FRAGMENTS WITH $1 \leq A \leq 14$ in 25 AND 15 MeV/NUCLEON REACTIONS

B.V. Jacak, G.D. Westfall, N. Anantaraman, M.W. Curtin, C.K. Gelbke, L.H. Harwood, B.E. Hasselquist, Z.M. Koenig, D.J. Morrissey, A.D. Panagiotou and D.K. Scott

Emission of light nuclear fragments has been studied for a large range of bombarding energies, from several MeV/nucleon through several GeV/nucleon. The production of such fragments can be understood in the framework of compound nuclear and deeply inelastic reactions in the low energy regime, and by emission from the fireball and fragmentation of projectile and target at high energies. The beams which have recently become available at the K500 Superconducting Cyclotron at MSU are in the energy region of several tens of MeV/nucleon, covering the transition from mechanisms typical of low bombarding energies to those of high energies. We have examined the systematics of light fragment (p-^{4}He) production[1]. However, for bombarding energies lower than 200 MeV/nucleon, measurement of light fragments alone is not sufficient. Heavier fragment at velocities intermediate between those of the projectile and target are also produced. The importance of measuring the heavy fragments is indicated in Fig.1, which shows the weighted average mass of the emitted particles with and without inclusion of fragments heavier than alpha particles. It is evident that the heavy fragments contribute significantly to the total emission of charged particles at bombarding energies less than 150 MeV/nucleon[2]. Formation of the heavy fragments drastically changes the number of degrees of freedom in the final state of the system[3], and measurement of the whole range of fragments is necessary to gain information on the nuclear equation of state. The bombarding energy dependence of fragment production may also yield information about possible phase transitions in nuclear matter[4].

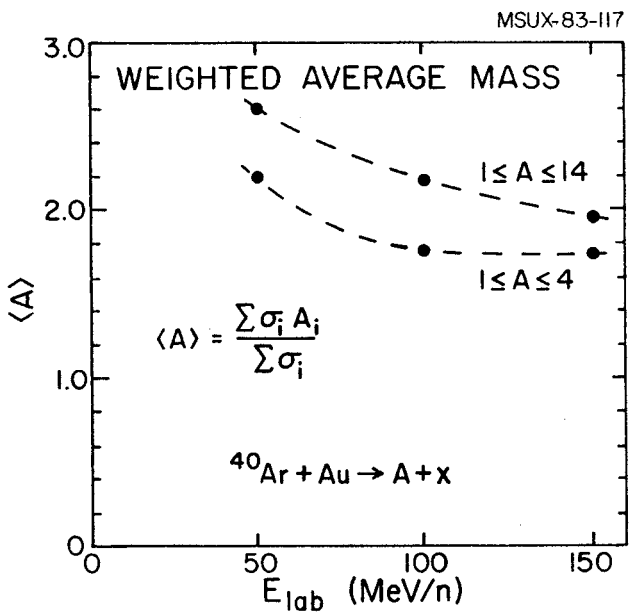

Fig. 1. The weighted average mass of emitted fragments from reactions of Ar + Au, as a function of bombarding energy. This plot shows the degree of clustering of charged particles. The importance of measuring nuclear fragments heavier than alpha particles at low bombarding energies ($E_{lab} < 50$ MeV/n) is evident.

Single particle inclusive energy spectra and angular distributions of fragments with $A \leq 14$ from a gold target were measured for 25 MeV/nucleon ^{4}He, ^{12}C and ^{22}Ne, and 15 MeV/n ^{22}Ne beams from the NSCL cyclotron. The angular distributions cover the range from 15 to 120 degrees in 15 degree steps. Midrapidity heavy ions were measured with two stacks of silicon detectors (0.1, 0.45, 5.0 mm and 0.8, 5.0, 5.0 mm) and low energy heavy ions with a telescope consisting of an ionization chamber ΔE backed by two silicon detectors. The ion chamber was run with 150 torr of 90% Ar - 10% methane gas, with an entrance window of 200 $\mu g/cm^2$ aluminum. The stopping detectors in the ion chamber telescope were each 0.4 mm thick. Isotopes for elements through carbon were well resolved in the silicon detectors, while elemental resolution through nitrogen was achieved in the ion chamber. Light particles (p,d,t,^{3}He,^{4}He and ^{6}He) were measured concurrently with a telescope made up of a 0.4 mm Si ΔE detector and a 4 inch NaI E detector.

Fig.2 shows a typical two-dimensional plot of ΔE vs. E for the thinner silicon telescope. The energy loss in the 0.45 mm detector is plotted as the y axis, and the stopping energy in the 5 mm detector is along the x axis. The separate lines are isotopes of helium, lithium, beryllium and boron. Particle identification is made by gating on these two-dimensional plots for each neighboring pair of detectors in the telescopes, and the energy spectra for lithium through nitrogen will result from joining the spectra from the three heavy ion telescopes. These energy spectra will range from just above the coulomb barrier to the energy of the projectile. The energy spectra and angular distributions will be fit with a single moving source model to determine the intermediate rapidity source temperature and velocity, and the total cross section for each particle. This experiment complements measurements of midrapidity fragments at higher energies[2,5,6], and will allow a systematic study of fragment production starting at energies where nuclear fragments arise primarily from deeply inelastic scattering to energies at which a participant-spectator approach is commonly accepted.

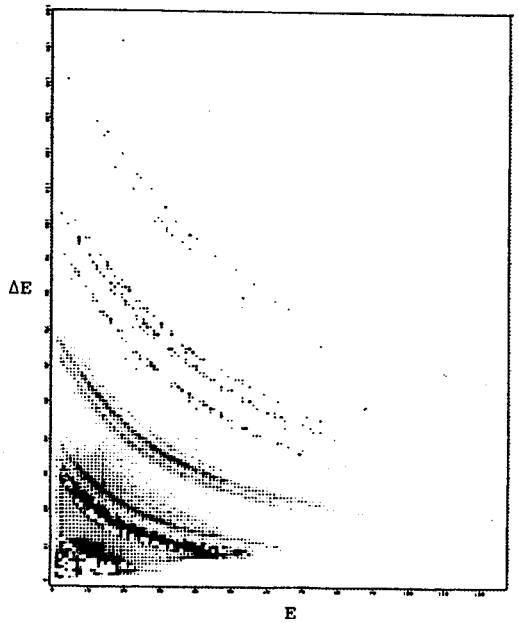

Fig. 2. A two dimensional plot of energy losses for particles stopping in the thin silicon telescope from the reaction of 25 MeV/nucleon 22Ne + Au. The energy loss in the 0.45 mm detector is plotted as the y axis, and the stopping energy in the 5 mm detector is along the x axis. The separate lines are isotopes of helium, lithium, beryllium and boron, illustrating the isotope resolution achieved with this telescope.

1. G.D. Westfall, B.V. Jacak, N. Anantaraman, M.W. Curtin, G.M. Crawley, C.K. Gelbke, B.E. Hasselquist, W.G. Lynch, D.K. Scott, M.B. Tsang, M.J. Murphy, T.J.M. Symons, R.Legrain and T.J. Majors Phys.Lett. 116B (1982) 118.
2. B.V. Jacak, G.D. Westfall, C.K. Gelbke, L.H. Harwood, W.G. Lynch, D.K. Scott, H. Stocker, M.B. Tsang and T.J.M. Symons, Phys. Rev. Lett. 51 (1983) 1846.
3. G. Bertsch and J.Cugnon, Phys.Rev. C24 (1981) 2514.
   H. Stocker, Lawrence Berkeley Laboratory Report 12302.
4. M.W. Curtin, H. Toki and D.K. Scott, Phys.Lett.123B (1983)289.
5. K.A. Frankel and J.D. Stevenson, Phys.Rev. C23 (1981) 1511.
6. J.Gosset, H.H. Gutbrod, W.G. Meyer, A.M. Poskanzer, A. Sandoval, R. Stock and G.D. Westfall, Phys.Rev. C16 (1977) 629.

FRAGMENTATION OF ^{14}N AT 30 MEV/U

L.H. Harwood, G.D. Westfall,
N. Anantaraman, B. Hasselquist,
B.V. Jacak, H. Utsunomiya, and A. Davenport

We have measured the longitudinal and transverse momentum distributions of the reaction products from $^{14}N+^{9}Be$ and $^{14}N+^{197}Au$ at 30 MeV/u. This was the first in a series of measurements intended to explore the velocity dependence of the widths of these distributions from 20 MeV/u to the upper limit of the NSCL facility. Above this range, data are available in the literature. There have been other similar experiments near 20 meV/u (see Ref. 1) but they suffered from not measuring both distributions but instead typically extract the longitudinal width by inspection of the energy spectrum at some fixed, large, (ie. greater than 15 deg.) scattering angle. Thus, the widths that they extract are somewhat influenced by the width of the transverse momentum distribution. We intend to extract the two widths with a two- dimensional Gaussian fit to our data; this will remove the interaction of the two widths that was present in the earlier studies.

This experiment was the first to use the S320 spectrograph to acquire nuclear physics data. We did not use it in its normal configuration, however. At the time of our experiment, two major experimental problems existed for trying to use the S320 in its normal configuration: 1) the focal plane detector system was not operational and 2) the time width of the beam was too large to allow complete particle identification of the heavier fragments we would observe. To overcome these problems, we substituted a Si counter telescope for the focal plane detector system; it gave us the particle energy directly and also identified the particles directly. The dispersion at the nominal focal plane position was sufficiently large that the detectors would only subtend a spread of 1% in momentum. The detectors were placed, therefore, on the port intended for transferring the beam to the split-pole spectrograph; the dispersion was a factor of 2 less at this point thereby making the detector subtend about 2 % in momentum. Particle rigidities from 0.7 to 1.15 of the beam rigidity were measured over the angular range 2-20 deg. Sample angular distributions are shown in fig. 1.

The large quantity of data acquired (approximately 240 separate runs) is now being processed. We can already see, however, by examination of the angular distributions in fig. 1 that the model which Van Bibber, et al (Ref. 2) used to fit their transverse momentum distributions

$$\sigma_{trans.} = \sigma_{long.}^2 + [A_f(A_f-1)/A_p(A_p-1)]\,\sigma^2_{trans.0}$$

would need a very small value of $\sigma_{trans.0}$ to be consistent with our data. A more specific result will be possible when all of the data is put together.

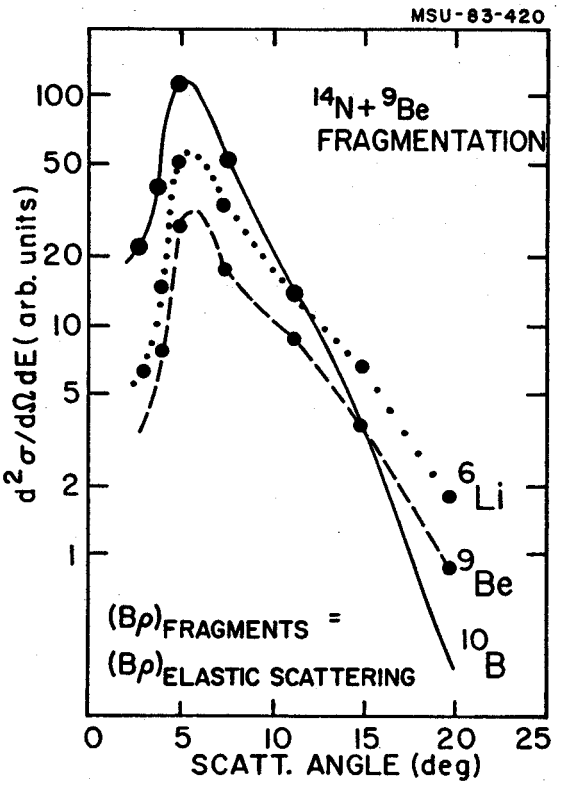

Fig. 1. Preliminary angular distributions for ^{14}N fragmention by ^{9}Be at 30 MeV/μ. Data for ^{6}Li, ^{9}Be and ^{10}B are shown. The observed particles had the same rigidity as elastically scattered beam particles.

1. M.J. Murphy and R.G.Stokstad, LBL Report 15188 (1983), (submitted to Phys. Rev. C) and references therin.
2. K. VanBibbe, et al., Phys. Rev. Lett. 43, 840 (197).

LIMITATIONS ON LINEAR MOMENTUM TRANSFER IN ^{14}N INDUCED REACTIONS ON ^{238}U AT E/A = 15, 20, 25, AND 30 MEV

M.B. Tsang, D.R. Klesch, C.B. Chitwood, D.J. Fields, C.K. Gelbke, W.G. Lynch, H. Utsunomiya, K. Kwiatkowski*, V.E. Viola, Jr.*, and M. Fatyga*

For nucleus nucleus collisions at energies well above the Coulomb barrier, the probability for complete fusion decreases markedly due to a rapid growth in fusion-like processes involving incomplete linear momentum transfer [1, 2]. Existing data on alpha conjugate projectiles indicate that the fraction of the projectile momentum transferred to the struck system decreases approximately linearly as the relative velocity of the projectile increases [1, 2]. Based on recent studies of ^{12}C induced reactions up to E/A = 84 MeV, it has been further suggested that there exists a saturation limit of about 2 GeV/c for the most probable linear momentum transfer for fusion-like events produced in heavy-ion collisions[3]. Up till now, little information exists for projectiles other than alpha conjugate nuclei which could provide some insight into the relative importance of nuclear structure to fusion-like intermediate energy heavy-ion induced reactions. To provide a more complete basis for evaluating the systematic projectile and bombarding energy dependence, linear momentum transfer distributions were measured in reactions between ^{14}N and ^{238}U at incident energies of E/A = 15, 20, 25, and 30 MeV.

The experiment was performed using ^{14}N beams from the K500 superconducting cyclotron of the National Superconducting Cyclotron Laboratory of Michigan State University. Linear momentum transfer distributions were determined by measuring the folding angles between coincident fission fragments using two position sensitive parallel plate detectors [4] of active area 12 cm x 14 cm. The centers of these detectors were positioned at the angles of θ_A°=70° and θ_B°=80° with respect to the beam axis and at a distance of 17 cm from the target. A UF_4 strip target of areal density of 0.4 mg/cm^2 and dimensions 3 mm x 22 mm, evaporated onto a 0.1 mg/cm^2 carbon backing was used. Absolute cross sections were obtained from the measurement of elastically scattered ^{14}N ions with two 1.5 mm thick monitor detectors positioned at the scattering angles of 8°.

Fission fragment folding angle distributions measured in this experiment are shown in Fig. 1. Here θ_A and θ_B denote the laboratory angles of the two coincident fission fragments measured with respect to the beam axis and $\Delta\Phi$ denotes the angle between the two planes defined by the beam axis in combination with either of the fission fragment

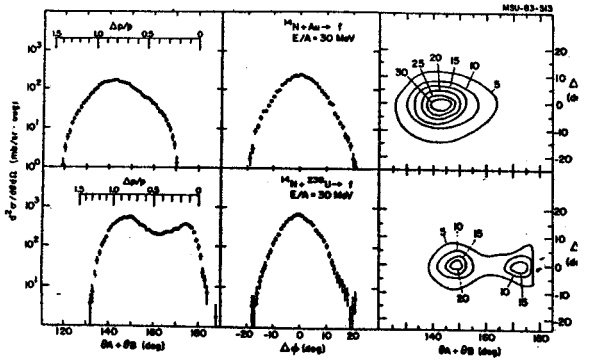

Fig. 1. Folding angle distributions between coincident fission fragments measured for ^{14}N induced reactions on ^{238}U at E/A = 15, 20, 25, and 30 MeV.

velocity vectors. In order to ensure full coincidence efficiency, these folding angle distributions were obtained by setting a gate on one of the fission detectors corresponding to an area of 2.4 x 2.4 cm^2 and an average scattering angle of θ_A= 86° for E/A=15 and 20 MeV and θ_A=83° for E/A=25 and 30 MeV. The right hand parts of the figure show contour plots of the number of coindident events in the $\theta_A + \theta_B$ vs. $\Delta\Phi$ plane. Two peaks corresponding to (i) large momentum transfer or fusion-like reactions, and (ii) small momentum transfer or peripheral reactions can be clearly distinguished.

The center column of Fig. 1 shows the out-of-plane distributions for the large momentum transfer reactions. For the ideal case of compound nucleus fission without light particle emission, two-body kinematics requires $\Delta\Phi$=0. Noncoplanar emission of fission fragments is caused by light particle emission which may occur either before or after the system fissions. As is evident from the figure, the widths of the out-of-plane distributions increase significantly with incident energy in accordance with an increase in the emission of light particles at higher energies.

The left hand parts of Fig. 1 show the dependence of the fission cross sections on the folding angle $\theta_{AB} = \theta_A + \theta_B$ which is related to the projection of the linear momentum of the fissioning nucleus onto the beam axis. The upper scales show the average recoil momentum Δp of the fissioning nucleus in units of the beam momentum p. This scale was established by assuming symmetric fission of ^{252}Es with a kinetic energy release corresponding to the systematics of ref. 14. Consistent with the observation for different projectiles [1] the large momentum transfer component cannot be understood in terms of

complete fusion followed by statistical decay. For higher projectile energies, smaller fractions of the projectile momentum are transferred to the fissioning nucleus, reflecting the increasing importance of non-equilibrium particle emission.

An upper limit for the contribution from complete fusion reactions to the total fission cross-section is obtained by assuming that complete fusion reactions can be represented by a Gaussian distribution in θ_{AB} with a width given by the measured $\Delta\Phi$ distribution for all fusion-like reactions. The relative contribution of complete fusion to the total fission cross-section decreases strongly with increasing beam energy, corresponding to $56^{+}5$, $42^{+}4$, $26^{+}4$, $21^{+}4\%$ for the incident energies of E/A=15, 20, 25 and 30 MeV, respectively. An extrapolation of the present data to higher energies suggests that complete fusion reactions will cease to contribute at incident energies above E/A = 40 - 45 MeV.

Figure 2 shows a compilation of most probable linear momentum transfers measured in reactions induced by various projectiles on actinide nuclei[1,2,5]. The energy dependence of the most probable linear momentum transfer measured in units of the projectile momentum is shown in Fig. 2a and the corresponding momentum transfer per projectile nucleon is shown in Fig. 2b. The fractional linear momentum transfer measured for ^{14}N induced reactions is seen to follow the systematic trends established [1] primarily for alpha conjugate projectile nuclei, indicating that the linear momentum transfer per nucleon depends primarily on the relative velocity of target and projectile and much less on the nuclear structure of the two colliding nuclei. At least for strongly absorbed projectiles of mass A=4-20, the individual nucleons appear to have comparable efficiency for transferring their momentum to the composite system.

There is evidence from both light ion and heavy ion induced reactions that the linear momentum transferred to the composite nuclear system reaches a maximum value at intermediate energies. For protons and deuterons maximum linear momentum transfer is achieved at E/A 1000 and 200 MeV, respectively [6]. For strongly absorbed ^{4}He projectiles maximum linear momentum transfer is achieved at lower energies, E/A 50 MeV [4, 6]. For ^{12}C induced reactions [4] the linear momentum transfer was suggested to reach a limiting value of Δp_{max} = 2GeV/c at bombarding energies above E/A = 15 MeV. For the present system, most probable momentum transfers in excess of 2 GeV/c are measured (Δp = 2.7 GeV/c at E/A = 30 MeV) and a limiting value is not reached below E/A = 30 MeV (see Fig. 2b). However, the results of refs. [4] and [6] suggest that one should expect the linear momentum transfer for the present system to saturate at incident energies in the range from E/A=30 to 50 MeV.

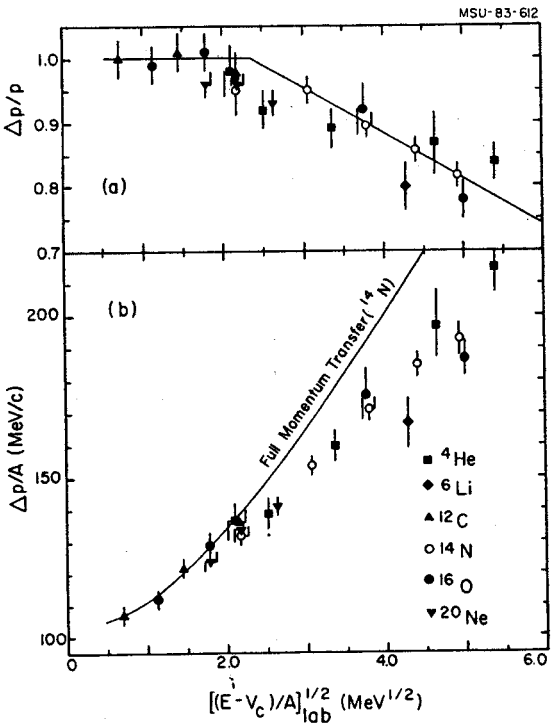

Fig. 2. Systematics of the energy dependence of the most probable linear momentum transfer measured in reactions induced by various projectiles on actinide target nuclei [1, 2, 5]. Part a shows the momentum transfer in units of the projectile momentum and part b shows the momentum transfer per projectile nucleon.

* Department of Chemistry and IUCF, Indiana University.

1. V.E. Viola, Jr., et al., Phys. Rev. C26 (9182) 178
2. Y. Chan, et al., Phys. Rev. C27 (1983) 447
3. J. Galin, et al., Phys. Rev. Lett. 48 (1982) 1787
4. J. Yurkon, et al., MSU Cyclotron Lab Annual Report 1981-82
5. M. Fatyga, private communication
6. F. Saint Laurent, et al., Phys. Lett. 110B (1982) 372

Li THERMOMETRIC MEASUREMENT OF NUCLEAR TEMPERATURE

D.J. Morrissey, W. Benenson, K. Beard, R.A. Blue,
E. Kashy, A.D. Panagiotou, R.M. Ronningen,
B. Sherrill, J. VanderPlicht, H. Utsunomiya

In nuclear reaction studies a temperature-like quantity is usually determined from the slope of the energy distribution of particles emitted by the nuclear system. Such descriptions of nuclear systems are readily accepted in compound nuclear reactions but are more tenous in high energy nuclear reactions. We have devised a method for measuring the temperature produced in the collision by observing the population of two level systems such as 7-Li. The population of the excited states of a system in statistical equilibrium depends on the temperature of the system and the energy level spacing. For a two level system at constant volume the dependence is simply the Boltzmann factor. For a nuclear system, such as 7-Li, we need to incorporate the statistical factors for the magnetic substates and any feeding from higher lying states and particle decay. This nucleus makes a particularly good probe for this method for three reasons: (1) there are no higher lying states and therefore it can not be fed from above, (2) the cross section for emitting successively heavier masses drops exponentially and feeding by particle decay should be negligible, and (3)the upper state decays by emitting an isotropic gamma ray. In figure 1 the calculated fraction of 7-Li nuclei that are in the excited state are shown as a function of temperature. The energy of the excited state is 477 keV and limits the sensitivity of the method to temperatures on the order of 2 MeV. If statistical equilibrium is really achieved, then a ratio of approximately 0.3 should be obtained in all reactions at temperatures above 2 MeV. Another useful nucleus is 6-Li which has six states up to 5.7 MeV only one of which gamma decays (the rest are particle unstable) The gamma emitting state at 3.562 MeV has a spin of 0+ and the spin factor in the Boltzman distribution gives the flat function in figure 1.

A preliminary test of the feasibility of the method was made at the NSCL k500 cyclotron with E/A=35 MeV 14N ions and a Ag target. Coincidences between Li ions emitted at 30 degrees and gammas detected in (a) 7.6 cm x 7.6 cm BGO at -150 degrees, or (b) an intrinsic Ge at +60 degrees, or (c) an intrinsic Ge at +120 degrees were recorded during a three shift run in the Gamma-ray beam line. The Li ions were detected in a Si solid state telescope which resolved the two isotopes. The energy spectrum of 7-Li was strongly peaked at approximately 30 MeV making the Doppler corrections straightforward. The results of the coincidence measurements give a near zero temperature which indicates that we have a mixture of evaporated fragments and directly emitted 7-Li nuclei. In the next operating period we hope to repeat the measurement at 90 degrees where the contributions from direct processes should be small. However, the results of this test run show the feasibility of checking the assumption of statistical equilibrium in nuclear reactions.

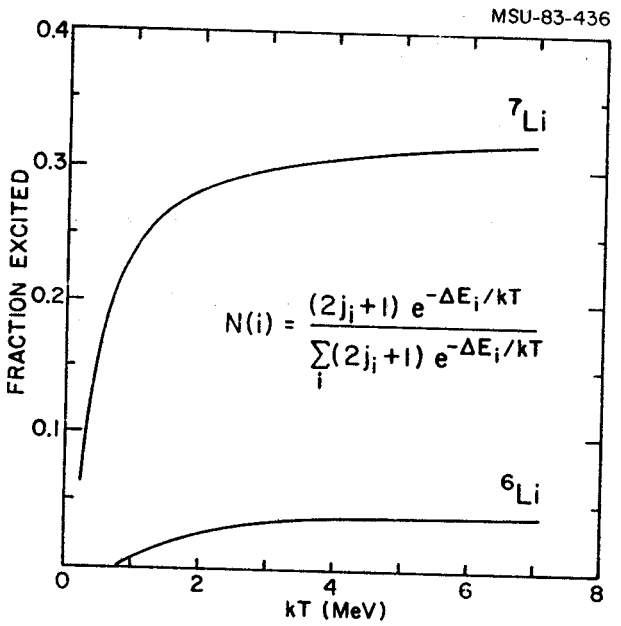

Fig. 1. The fraction of Li nuclei expected to be in their gamma emitting excited states is shown as a function of temperature.

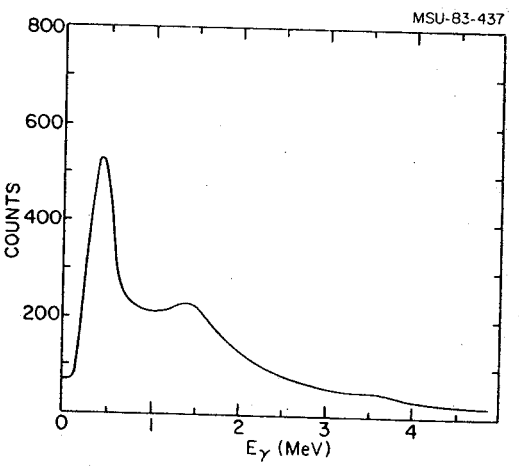

Fig. 2. A portion of the gamma-ray spectrum in coincidence with Li ions is shown. The Doppler shifted gamma-ray connecting the excited and ground states of 7-Li is clearly visible at 435 keV.

COMPLETE AND INCOMPLETE FUSION REACTIONS

D.G. Kovar*, R. Janssens*, G.S. Stephans*,
G. Rosner*, H. Ikezoe*,
B. Wilkins*, C.K. Gelbke, B.V. Jacak, Z.M. Koenig,
and G.D. Westfall

For many years the fusion channel has been a focal point for heavy ion reactions and has been of critical importance in characterizing such factors as angular momentum cutoffs, nuclear structure effects, and nuclear dynamics[1-3]. The measurement of evaporation residues provides an unique signature for the fusion channel, at least for low entrance channel energies. As bombarding energies are increased above 15 MeV/nucleon, non-equilibrium emission of fast particles becomes a prominent mechanism and the measurement of evaporation residues becomes informative. A variety of models such as hot spots, Fermi jets, and PEPS have been proposed but there has been a lack of systematic experimental studies for comparison.

The measurements to study these phenomena were carried out with beams of 15, 25, and 35 MeV/nucleon ^{14}N incident on five targets including ^{12}C, ^{24}Mg, ^{27}Al, ^{48}Ti, and ^{58}Ni. Evaporation residues of fusion reactions were studied in the 60" scattering chamber using a time-of-flight telescope consisting of two microchannel plate detectors and a silicon total energy detector. To gain sufficient flight path for the residues, the targets were placed near the entrance of the chamber and the detectors were placed on an arm that pivoted at the target position and moved to angles in the range of 0.5 to 5° in the laboratory. The long flight path combined with the time resolution of 100 psec gave good mass resolution for all residues observed.

Analysis is in progress.

---

* Argonne National Laboratory

1. B.B. Back, K.L. Wolf, A.C. Mignerey, C.K. Gelbke, T.C. Awes, H. Breuer, V.E. Viola, and P. Dyer, Phys. Rev. C22, 1927 (1980).
2. P. Gonthier, H.Ho, M.N. Namboodiri, L. Adler, J.B. Natowitz, S. Simon, K. Hagel, R. Terry, and A. Khodai, Phys. Rev. Lett. 44, 1387 (1980).
3. H. Morgenstern, W. Bohne. K. Grawisch, D.G. Kovar, and H. Lehr (to be published) and D.G. Kovar, W. Bohne, M. Bürgel, Ch. Egelhaaf, M. Fuchs, A. Gamp, K. Grawisch, D. Milscher, M. Homeyer, H. Morgenstern, and W. Rauch, Bull. Am. Phys. Soc. 26, 1133 (1981).

NEUTRON EMISSION IN DEEP-INELASTIC SCATTERING OF ^{14}N ON ^{165}HO AT 35 MEV/NUCLEON

G. Caskey*, F. Deak**, A. Galonsky*, C.K. Gelbke*, J. Hinnefeld***, A. Kiss**, J.J. Kolata***, B. Remington*, Z. Seres+ and M.B. Tsang*

Previous studies of light-particle emission in heavy-ion reactions have focused on energies below 20 MeV/n or above 1 GeV/n, leaving a paucity of data between. The intervening energy range is of interest however because 20 MeV/n roughly marks where the collision speed approaches the average speed of nucleons inside a nucleus: the Fermi velocity. Below E/A = 20 MeV, equilibrium processes dominate owing to the long interaction time, with pre-equilibrium processes becoming more important as the energy increases.[1] The emitted radiations bear the signatures of their creation and can, in principle, give clues to the reaction mechanism(s). By studying neutron emission in deep-inelastic heavy-ion scattering we avoid coulomb effects on the emission spectra and at 35 MeV/n we can study an interesting energy region. Our objective is to make exclusive measurements of neutrons in coincidence with light (projectile-like) fragments in deep-inelastic heavy-ion reactions above E/A = 20 MeV.

The target, a 7.6 mg/cm^2 foil of ^{165}Ho, was bombarded with a 490 MeV $^{14}N^{5+}$ beam from the K500 cyclotron at MSU. Light fragments (LFs) were identified by three silicon ΔE-E type telescopes at θ_{lab} = 10° and -30° in the horizontal plane and at θ_{lab} = 30° below the beam. Ten NE213 scintillation counters were arrayed at θ_{lab} = ±10°, ±30°, -45°, ±60°, ±90° and -110° in a geometry coplanar with the two LF telescopes in the horizontal plane. Typical target-to-detector flight paths were 1.6 m for the scintillation counters. At 30° below the beam, one LF telescope allows observing out-of-plane neutron emission for all ten polar angles. Details of the neutron chamber and beam line used for this experiment are in Ref. 2.

Neutron energies were measured by time-of-flight (TOF) of the neutron relative to the light-fragment (LF) detection time, then corrected for the LF-TOF. The n-γ discrimination technique was employed for neutron identification.

An event record was constructed if one or more LF telescopes fired in coincidence with one or more neutron (scintillation) detectors. The ΔE, E, and time for the light fragment detectors together with the neutron TOF, n-γ discrimination signal and light output for the neutron detectors were recorded for all detectors which were in coincidence in any event. LF singles spectra were also recorded.

MSU-83-482

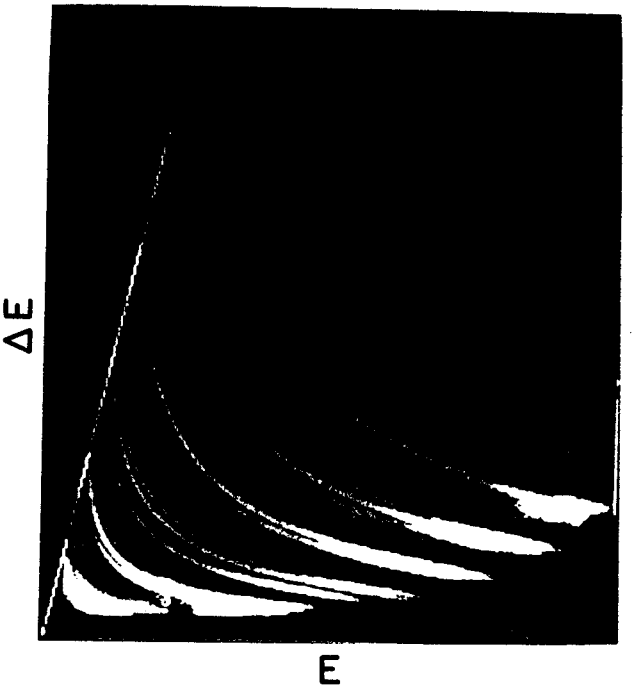

Fig. 1. ΔE-E spectrum for the θ_{lab} = +10° LF telescope. Note the isotopic separation in the Li, Be and B bands, especially at lower energies.

Figure 1 shows a ΔE vs E plot for the θ_{lab}=10° LF telescope. Note the effective isotopic separation for, e.g., beryllium, particularly at the lower energies. Alpha particles and (quasi) elastic nitrogen dominate this spectrum.

A few neutron TOF spectra appear in figure 2 for neutrons in coincidence with a LF in the θ_{lab}=10° LF telescope. These spectra are not corrected for detector efficiencies or thresholds, background or for accidental coincidences but are corrected for LF-TOF. The γ-ray peak has a FWHM < 1ns evidencing good time resolution. Neutrons appear in two groups, one seemingly a typical low energy evaporation curve while the other is peaked at energies somewhat below the beam energy. This second peak diminishes rapidly as one goes to back angles. Compare, for example, the spectra at θ_{lab}=10° and 90° in Figure 2.

Analysis of the data is presently underway and will involve further work at MSU and in Budapest.

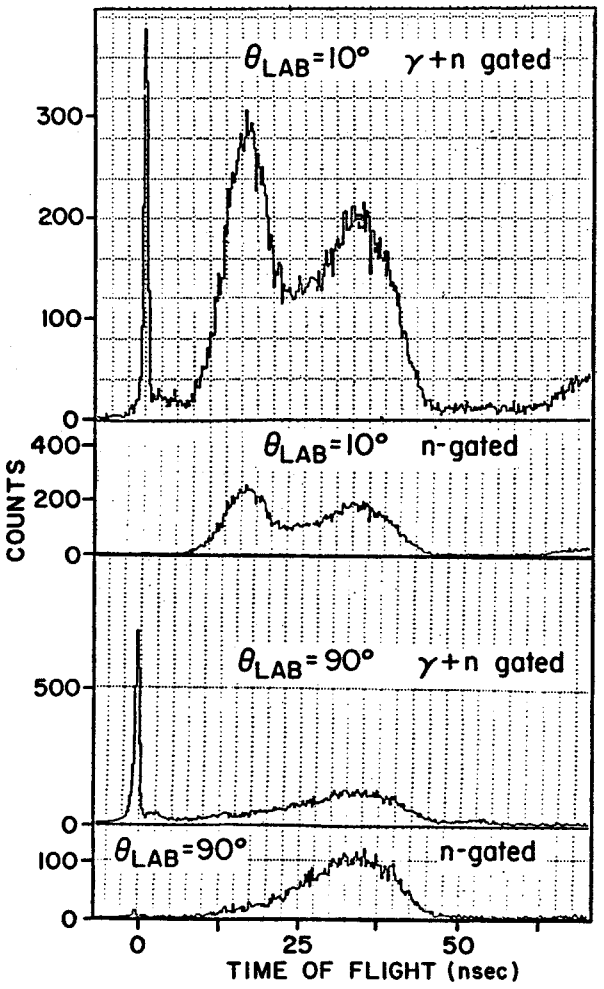

Fig. 2. Time-of-flight spectra for scintillation counters at θ_{lab}=10° and 90°, in coincidence with a LF in the θ_{lab} = 10° telescope. One spectrum at each angle is ungated and below each of these is the same spectrum gated on neutrons. Note the double peaked structure in the neutron portion of the spectra. (Software light thresholds were set at the ThC" compton edge, namely about 2.4 MeV electron energy, for these spectra).

* Cyclotron Laboratory, Michigan State University, E. Lansing, MI.
** Eötvös University, Budapest, Hungary.
\+ Central Research Institute for Physics, Budapest, Hungary.
*** Notre Dame University, Notre Dame, IN.

1. C.K. Gelbke, C. Olmer, M. Buenerd, D.L. Hendrie, J. Mahoney, M.C. Mermaz and D.K. Scott, Phys. Rep. 42 (1978) 311.
2. B. Remington, et.al., Section F of this report.

TWO-PARTICLE INCLUSIVE MEASUREMENTS OF NON-COMPOUND LIGHT PARTICLE EMISSION IN NUCLEUS-NUCLEUS COLLISIONS

W.G. Lynch, C.B. Chitwood, M.B. Tsang, D.J. Fields, D.R. Klesch, C.K. Gelbke, A.D. Panagiotou, G.R. Young*, T.C. Awes*, R.L. Ferguson*, F.E. Obenshain*, F. Plasil* and R.L. Robinson*

Nonequilibrium particle emission in intermediate-energy nuclear collisions is a phenomenon whose description presents a clear challenge to our current understanding of nuclear reactions . Of the many differing theoretical approaches, the concept of a spatially localized region of high excitation ("hot spot")[1-4] has received support from the comparisons of inclusive light particle spectra and multiplicities with statistical predictions.[5,6] While these comparisons test the thermal assumptions of the "hot spot" picture, until now the particular aspect of spatial localization has lacked direct experimental verification. Here we report results from two-proton correlation measurements that provide evidence for particle emission from a spatially localized region of high excitation in qualitive agreement with the concept of a "hot spot".

The experiment was performed at the Holifield Heavy Ion Research Facility. A gold target of 8.6 mg/cm^2 was bombarded with ^{16}O ions of 400 MeV incident energy. Single and coincident protons were detected with 13 ΔE-E-telescopes consisting of silicon ΔE- and NaI E-detectors. Small angle correlations were measured with six telescopes with individual solid angles of 0.76 msr. The detectors were mounted in a closely packed hexagonal array that was centered at the scattering angle of 15°. The angular resolution and the angular separation between adjacent telescopes were 1.6° and 5.1°, respectively. Large angle correlations were measured with seven telescopes of solid angles between 13 and 41 msr. Three of these telescopes were mounted in the plane of the small angle hodoscope (ϕ=0°) at the scattering angles of θ=40°, 70°, and 130°, where θ and ϕ denote the polar and azimuthal angles measured with respect to the beam axis. The remaining four telescopes were positioned at the polar angles of θ= 40°, 70°, 130°, and 160°; their azimuthal angle was varied between 50° and 180°. Absolute cross sections, accurate to 10%, were obtained from the integrated beam current, the target thickness and the solid angles of the telescopes. Energy calibrations accurate to 3% were obtained by measuring the energies of recoil protons backscattered from a Mylar target by a 200 MeV ^{16}O beam.

Consistent with previous observations, the singles light-particle cross sectons are rather well described in terms of thermal emission from a hot source of nucleons having an apparent temperature considerably higher than that of the compound nucleus and moving with slightly less than half the beam velocity[6]. Comparisons of the one- and two-particle energy spectra and angular distributions do not reveal any strong dynamical correlations in the two particle data[7] which suggests that the one- and two-particle data share a common production mechanism consistent with a thermal interpretation.

Information regarding the space-time extent of the emitting source is contained in the magnitude of the final state correlations between light particles emitted at small relative momenta. For the case of two protons emitted at close proximity in space and time, the strong attractive nuclear interaction in the singlet s partial wave causes a characteristic enhancemant in the two-proton correlation at relative momenta of about 20 MeV/c.[8] Emission from a source of large dimensions or long source lifetimes will result in a reduced final state effect. Measurements of two proton correlations at small relative momenta have been used to determine the size of the nuclear fireball at relativistic beam energies[9].

The two-proton correlation function, $R(p_1,p_2)$, is defined in terms of the singles cross sections, $\sigma(p_1)$, $\sigma(p_2)$ and coincidence cross sections $\sigma(p_1,p_2)$, by

$$\sigma(p_1,p_2) = C\sigma(p_1)\sigma(p_2)(1 + R(p_1,p_2)) \qquad (1.)$$

where the p's denote the proton momenta and the normalization constant C is experimentally determined by the condition $R(p_1,p_2)=0$, for sufficiently large relative momenta, where final state interactions are not important. For a source of negligible lifetime, $R(p_1,p_2)$ depends principally upon the magnitude of the relative momentum $\Delta p=|p_1-p_2)|/2$.[8] The experimental correlation function, shown in fig. 1, was obtained by inserting the cross sections, measured with the small angle hodoscope, into Eq. 1 and by summing both sides of the equation over all energies and angles corresponding to a given relative momentum. The curves shown in the figure are the results of model calculations[8] for the case of incoherent emission from a source of negligible lifetime and gaussian spatial distribution of rms radius $\sqrt{3/2}\ r_o$. The correlations observed experimentally are slightly larger than those calculated for a source with r_o = 4 fm. Nonnegligible decay times will reduce the correlations, therefore values for r_o deduced by comparison with the present calculations represent upper limits on the average source sizes.

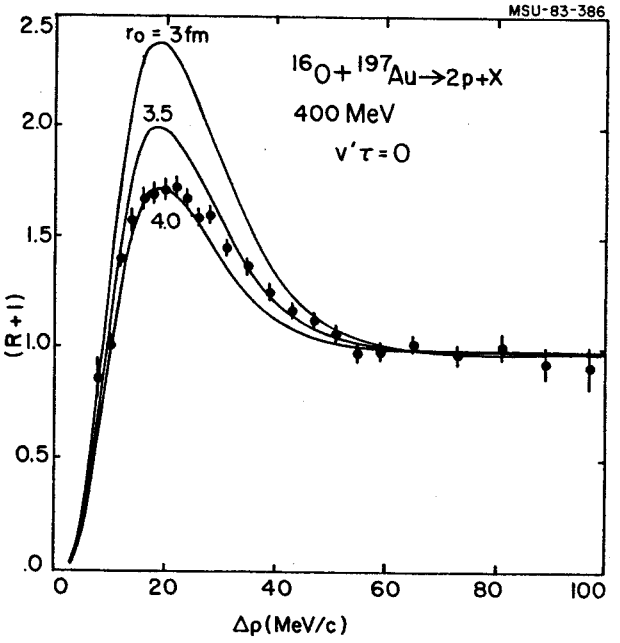

Fig. 1. The experimental correlation function 1 + R(Δp) is plotted as a function of the proton relative momentum. The errors are purely statistical. See the text for a discussion of the curves.

Further insight may be gained by investigating the dependence of the measured correlation function 1+R(Δp) on the total energy of the two coincident protons. This energy dependence is shown in Fig. 2 for the relative momentum intervals of $\Delta_1 p$ = 15-25 MeV/c (where R(Δp) is predicted to reach a maximum) and $\Delta_2 p$ = 50-80 MeV/c (where R(Δp) is predicted to be negligible). For the lowest proton energies, no substantial differences in the correlations of the two momentum intervals are observed, which indicates that these protons are predominantly emitted from a source of rather large space time extent, e.g. a long lived compound nucleus. With increasing proton energies the differences between the measured correlations become more pronounced, which indicates that high energy protons are emitted primarily from a short - lived and spatially localized region of high excitation, in qualitative agreement with the concept of formation and decay of a "hot spot". For proton energies above E1+E2=90 MeV the ratio $(1+R(\Delta_1 p))/(1+R(\Delta_2 p))$ yields an upper limit of r_o=3.1 fm. With the assumption that the gaussian source has a central density of normal or twice nuclear matter density (.015fm^{-3}), a maximum number of 25 or 50 participating nucleons is estimated, respectively.

In fig. 3, the correlation function corresponding to Δp = 50-80 MeV/c decreases slightly for increasing energy of the coincident protons. This decrease may be understood in terms of the phase space constraints imposed by energy and momentum conservation. In order to assess these effects, we assume for simplicity that only a subset of nucleons have interacted strongly during the time in which the two protons are emitted. These protons are assumed to be emitted isotropically with a Maxwell-Boltzman distribution in the rest frame of this subset of nucleons. Following the emission of the first proton the subset recoils with a recoil velocity

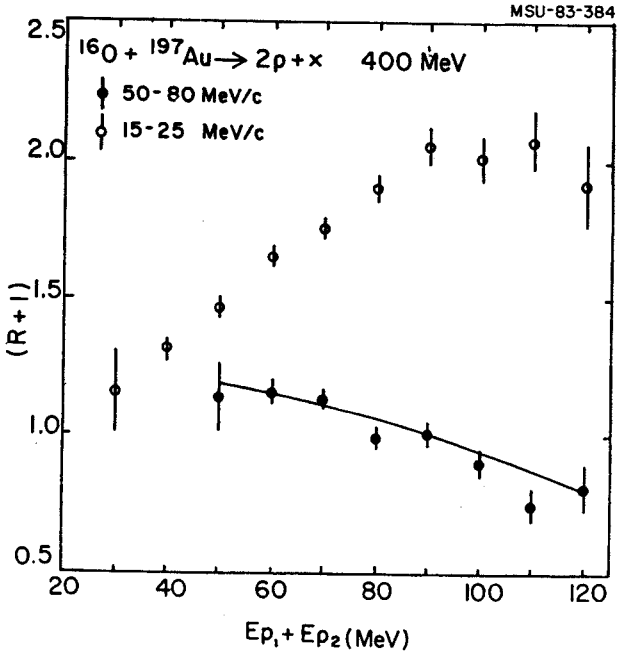

Fig. 2. The correlation function 1 + R(Δp), gated on relative momentum intervals of 15-25 MeV/c and 50-80 MeV/c, is plotted as a function of the sum energy of the two protons. The errors are purely statistical. See the text for a discussion of the solid line.

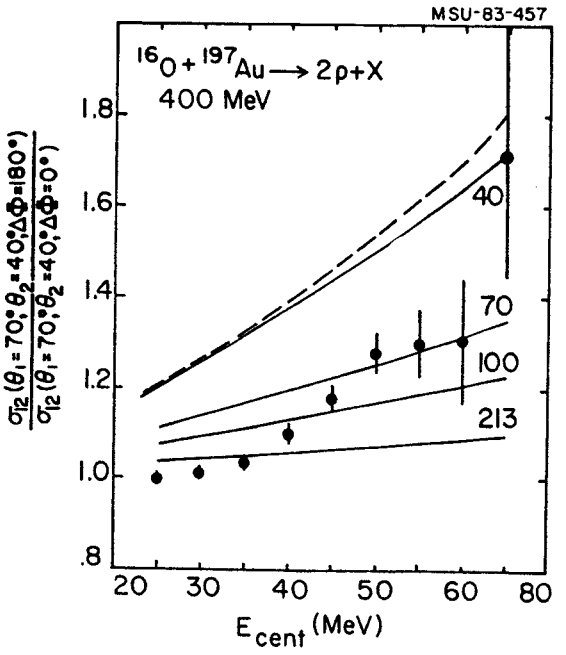

Fig. 3. The ratio of the energy-integrated coincidence cross section for Δφ = 180° to that of Δφ = 0° is plotted as a function of the midpoint of the integration interval of 20-MeV width. The errors are purely statistical. See text for a discussion of the curves.

defined by momentum conservation and the number of nucleons in the source, A_s.[7] This moving-source parameterization provides an adequate description of the inclusive data[6] and is consistent with the overall features of the coincidence data.[7] The solid line in Fig. 2 shows the correlation expected for a subset with apparent temperature of 7.1 MeV and average velocity of .067c consisting of A_s = 40 nucleons.

The phase space constraints imposed by momentum conservation may be used to assess the number of participating nucleons. Since the singles and coincidence cross sections depend strongly on the polar emission angle, these phase space constraints are best demonstrated by fixing the polar angles of the coincident protons and examining the ratio of cross sections for coplanar emission on opposite sides ($\Delta\Phi$=180°) to coplanar emission on the same side of the beam axis ($\Delta\Phi$=0°). In fig. 4, this ratio is shown for the polar angles of θ_1=40° and θ_2=70°. For each data point of the figure, the cross sections have been integrated over an identical energy interval of 20 MeV width for each proton. The cross section ratio is plotted at the midpoint of this interval.

The correlations expected from momentum conservation with subsets consisting of A_s = 40, 70, 100, and 213 nucleons are shown by the solid curves in Fig. 3. These calculations were performed by assuming a fixed temperature of 7.1 MeV. (If one adopts a consistent thermal interpretation of this moving source parameterization, the emission of the first proton should cool the source. The effect of cooling was assessed for the case of A_s=40, see the dashed curve in Fig. 3. It can be seen from the figure that the energy conservation requirement has only a small effect on the asymmetry.) Since rescattering by any nearby cold nuclear matter can reduce the asymmetry expected for the smaller subsystems, estimates of A_s deduced by comparisons of data to these calculations can be viewed as upper limits to the number of strongly interacting nucleons. For low energy protons, the experimentally observed asymmetry is small and comparable to the calculation for 213 nucleons (the compound nuclear mass). For protons of higher energy, however, considerably larger asymmetries are observed corresponding to significantly smaller source sizes. This trend is in qualitative agreement with our conclusions from the analysis of the small angle correlations.

In summary, two proton correlations measured for ^{16}O induced reactions on ^{197}Au at 400 MeV provide evidence for the formation and decay of a localized region of high excitation in agreement with the physical picture of a "hot spot". High energy protons sample the early stages of the reaction characterized by a rather small space-time extent of the emitting source. Low energy protons, on the other hand, are primarily emitted at later stages of the reaction corresponding to an emitting source consistent with the compound nucleus.

* Oakridge National Laboratory, Oakrdige, TN.

1. H.A. Bethe, Phys. Rev. 53, 675 (1938).
2. R.Weiner and M. Westrom, Nucl. Phys. A286,282 (1977).
3. S.I.A. Garpman, D. Sperber, and M. Zielinska-Pfabe, Phys.Lett. 90B,53 (1980).
4. S.I.A. Garpman et al., Phys. Lett. 92b,56 (1980).
5. C.K. Gelbke, Comments Nucl. Part. Phys. 11, 259 (1983), and references given therein.
6. T.C. Awes, et al., Phys. Rev. C25, 2361 (1982).
7. W.G. Lynch, et al., Phys Lett. 108B, 274 (1982).
8. S.E. Koonin, Phys. Lett. 70B, 43 (1977).
9. F. Zarbakhsh, et al., Phys. Rev. Lett. 46, 1268 (1981).

NEUTRON AND GAMMA RAY EMISSION FOLLOWING $^{16}O + ^{12}C$ FUSION

B. Remington, P. DeYoung*, A. Galonsky, F. Haas**, J.J. Kolata*, F. Prosser+, R. Racca+ and L. Sathoviac*

A series of experiments has been completed on the tandem Van de Graaff accelerator at Notre Dame to locate the entry lines in the residues from fusion of ^{16}O with ^{12}C at seven center-of-mass (CM) energies from 20 to 26 MeV. Average gamma multiplicity and energy were measured, thus, with an assumption about the average angular momentum carried off by each, a determination of the entry point of the residue on an Yrast diagram can be made (see Fig. 1). As a cross-check on the energy coordinate, the average energy carried off by the particles which precede gamma ray emission has also been measured. The work on neutron energy is described here.

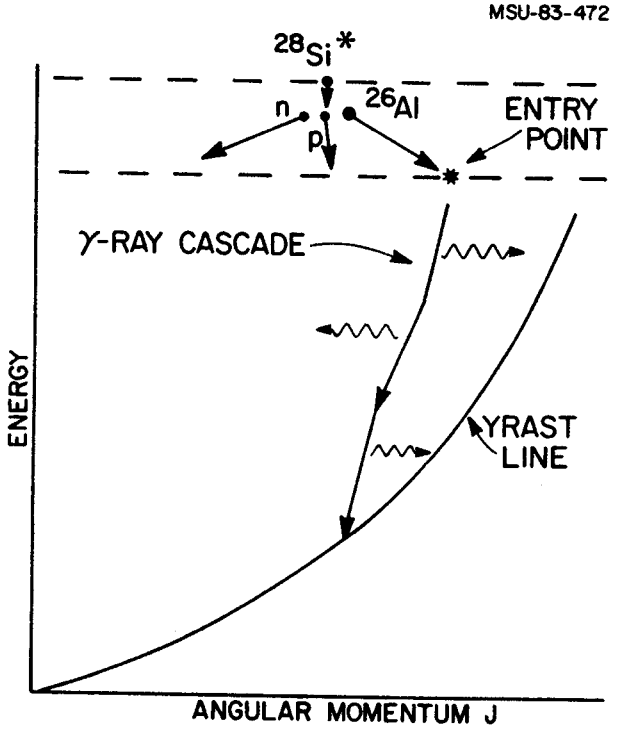

Fig. 1. $^{28}Si^*$ breaks up into n,p, and $^{26}Al^*$. Then $^{26}Al^*$ de-excites by gamma ray emission. For an average gamma multiplicity and energy and an assumed average angular momentum, the entry point can be determined.

We placed six neutron detectors around the target at various angles and a Ge(Li) detector at 125° to the beam and recorded gamma-neutron coincidence events on magnetic tape. Gamma peaks in the neutron-gated spectra were seen for ^{26}Al, ^{25}Mg, and ^{23}Mg residues (see Fig.2), and for each peak and beam energy the neutron data were sorted into time-of-flight (TOF) spectra. Fig. 3 shows one of roughly 550 such spectra. This was for the neutron detector at 0° to the beam direction, gated on the 830 KeV gamma line of ^{26}Al, at lab ^{16}O energy of 50.8 MeV. These TOF spectra were then transformed into energy spectra in the lab frame (see Fig. 4) and then into the CM system as defined by the ^{28}Si compound nucleus (see Fig. 5). The spectrum in Fig. 5 is fitted with an evaporation spectrum with a Gaussian resolution function of FWHM=4ns folded in at the TOF level. A CM evaporation spectrum of the following form was assumed.

$$N(E) = K\sqrt{E}\, e^{-E/T}$$

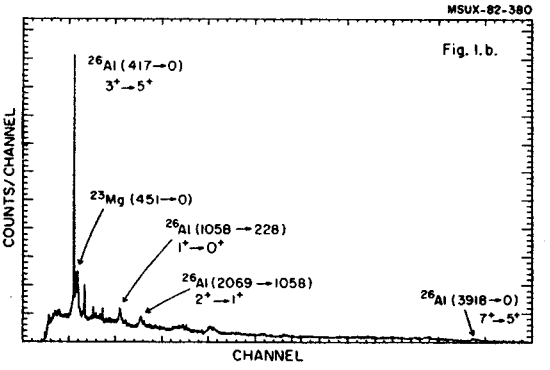

Fig. 2. The neutron-gated Ge(Li) spectrum for a beam energy of 50.8 MeV. Five of the observed nine peaks for ^{26}Al, ^{25}Mg, ^{23}Mg residues are indicated.

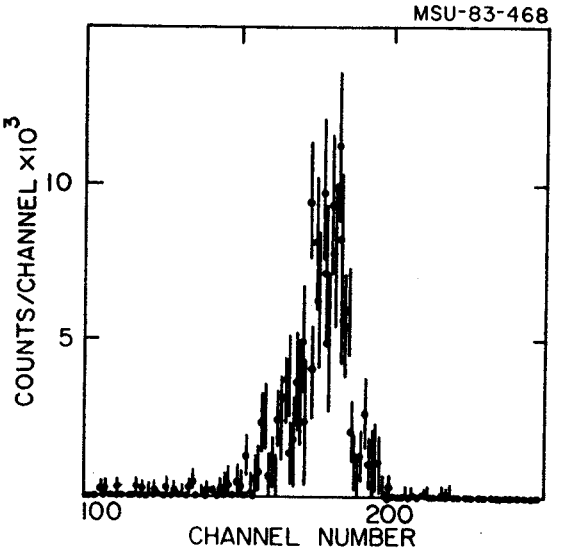

Fig. 3. The time-of-flight (TOF) spectrum from the 0° neutron detector detector gated on the 830 KeV gamma ray from ^{26}Al and at beam energy of 50.8 MeV.

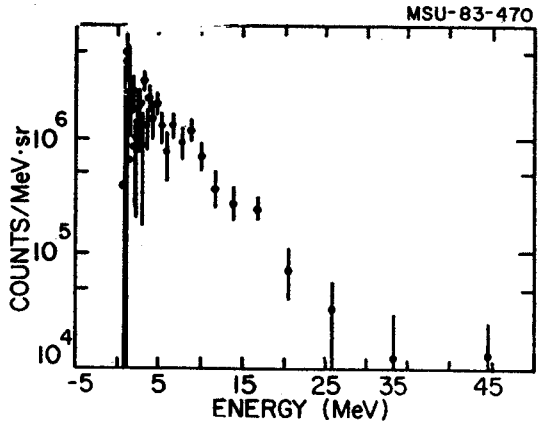

Fig. 4. The lab energy spectrum for the TOF spectrum in Fig. 3.

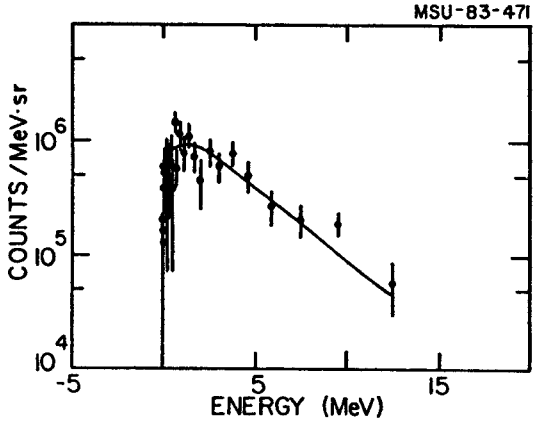

Fig. 5. The CM energy spectrum for the lab energy spectrum of Fig. 4. The fit is for an evaporation spectrum with T=2.52 MeV.

The next step in the analysis was to determine average neutron energy in the CM system for each beam energy and residue. Since

$$\langle E \rangle = \frac{\int\int d\Omega\, dE\, E\, N(E,\theta)}{\int\int d\Omega\, dE\, N(E,\theta)}$$

we have to know the angular dependence (in the CM system) of neutron emission. By utilizing the angular distribution obtained with our six neutron detectors, we can in essence fix E and vary θ, thus examining the θ dependence of $N(E,\theta)$. One example is displayed as Fig. 6. Many such plots were produced, none of which showed any consistant anisotropy about $\theta=90^{\circ}$. The assumption we made was that the neutron emission is isotropic in the CM frame, thus simplifying the integral for $\langle E \rangle$. The results obtained are displayed in Table 1. Still remaining to be done in this analysis are the following:

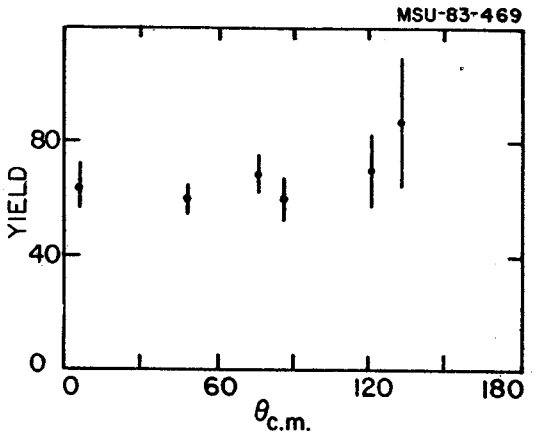

Fig. 6. Neutron yield $N(E,\theta)$ vs θ for a fixed energy bin of 3-5 MeV.

1. The uncertainties presented for each $\langle E \rangle$ do not yet account for the finite time, and therefore energy, resolution of our detectors.
2. A correction to $\langle E \rangle$ itself results from the finite time resolution of our detectors, and this has not yet been added in.
3. The neutron analysis and charged particle analysis have to be combined to produce the average energy carried away by particle emission, thus checking our entry line determination. The charged particle analysis is being carried out at Notre Dame.

Table 1. Average neutron energies for the various beam energies, Ge(Li) orientations, and residues. "Ge(Li) opp." means the Ge(Li) detector was on the opposite side of the beam direction as the neutron detectors, and "Ge(Li) same" means it was on the same side as the neutron detectors. More beam energies were run in the "Ge(Li) opp." configuration than in the "Ge(Li) same" configuration.

Residue	Beam Energy(MeV)	Ge(Li) opp. $\langle E \rangle \pm \Delta\langle E \rangle$ in MeV	Ge(Li)same $\langle E \rangle \pm \Delta\langle E \rangle$ in MeV
^{26}Al	43.2	3.42 ± .08	3.08 ± .07
	46.0	3.57 ± .08	3.41 ± .08
	48.3	3.92 ± .10	4.06 ± .10
	50.8	3.21 ± .07	
	53.7	4.45 ± .13	
	56.0	4.55 ± .19	4.46 ± .13
	60.7	4.45 ± .13	
^{25}Mg	50.8	3.70 ± .35	
	53.7	3.36 ± .25	
	56.0	3.95 ± .46	4.28 ± .30
	60.7	3.74 ± .15	
^{23}Mg	43.2	2.52 ± .17	2.58 ± .14
	46.0	2.75 ± .18	2.73 ± .16
	48.3	3.09 ± .15	2.98 ± .16
	50.8	2.49 ± .13	
	53.7	3.15 ± .13	
	56.0	4.46 ± .24	3.44 ± .12
	60.7	2.64 ± .08	

* University of Notre Dame
** University of Kansas
+ Centre de Recherche Nucleaires Strasbourg, France

ENERGY DEPENDENCE OF FISSION FRAGMENT ANGULAR DISTRIBUTIONS FOR ^{19}F, ^{24}Mg, ^{28}Si, AND ^{32}S INDUCED REACTIONS ON ^{208}Pb

M.B. Tsang, D. Ardouin[+], C.K. Gelbke, W.G. Lynch, H. Utsunomiya, Z. Xu[++], B.B. Back[*] S. Saini[*], P.A. Baisden[**], and M.A. McMahan[**]

In order to obtain more information about the systematic trends of fission fragment angular distributions observed in heavy ion induced reactions, we investigated ^{19}F, ^{24}Mg, ^{28}Si induced reactions on ^{208}Pb over the range of incident energies of E/A = 5.6 - 10 MeV. A similar study on ^{32}S + ^{208}Pb system has been reported in last year annual report.

The experiment was performed at the superconducting linear postaccelerator at Argonne National Laboratory. A ^{208}Pb target of 0.2 mg/cm^2 areal density was used. Except for the larger number of detectors used in the present experiment, the experimental technique was identical to the one described in last year annual report. The fission fragment angular distributions measured in the present experiment are shown in Figure 1. Similar to previous measurements for ^{32}S induced reactions on ^{208}Pb reported last year, larger angular anisotropies are observed at higher incident energies.

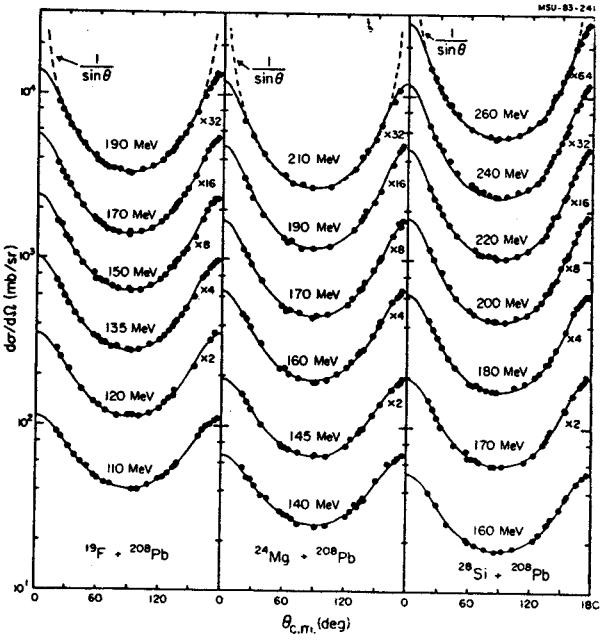

Fig. 1. Fission fragment angular distributions measured for ^{19}F, ^{24}Mg, and ^{28}Si induced reactions on ^{208}Pb. The solid curves are the result of the global fits in terms of equations 1-4. The dashed lines show the limit of $d\sigma/d\Omega = 1/\sin\theta$.

We assume that the final helicity distribution of the fission fragments reflects a statistical equilibrium distribution at some intermediate stage of the reaction; this "transition state" is generally identified with the saddle point[1] if the reaction proceeds via formation of an equilibrated compound nucleus. For first chance fission following the capture of spin - zero projectile and target nuclei, the expression for the angular distributions is given by

$$\frac{d\sigma}{d\Omega}(\theta) = \pi\lambda^2 \sum_{\ell=0}^{\infty} (2\ell+1)\, T_\ell \; \frac{\sum_{K=-\ell}^{+\ell} \frac{1}{2}\,(2\ell+1)\,|D^{\ell}_{M=0,K}(\theta)|^2 \exp\left(-\frac{K^2}{2K^2_{0,\ell}}\right)}{\sum_{K=-\ell}^{+\ell} \exp(-K^2/2K^2_{0,\ell})} \qquad (1)$$

with

$$K^2_{0,\ell} = T\mathcal{J}_{eff}/\hbar^2 = T\left(\frac{\hbar^2}{\mathcal{J}_{\parallel}} - \frac{\hbar^2}{\mathcal{J}_{\perp}}\right)^{-1} \qquad (2)$$

Here, T_ℓ denotes the probability of capture for the partial wave of angular momentum ℓ, $D^{\ell}_{M=0,K}$ is the symmetric top wave function, T is the nuclear temperature, and $\mathcal{J}_{\parallel}$ and $\mathcal{J}_{\perp}$ are the transition state moments of inertia about axes of rotation parallel and perpendicular to the symmetry axis.

Fission fragment angular distributions at energies close to the fusion barrier depend strongly on the distribution of the partial wave fusion probabilities T_ℓ, as discussed in detail in ref. 2. For the fits shown by the solid curves in Figure 1, we have used the relation[2,3]

$$T_\ell = T^{(OM)}_{\ell+\ell'} \qquad (3)$$

where $T^{(OM)}_\ell$ are transmission coefficients obtained from optical model fits to elastic scattering angular distributions that were simultaneously measured in this experiment. At each energy the parameter ℓ' was adjusted to reproduce the experimental fission cross section. The angular momentum dependence of the effective moments of inertia was parameterized by the simple functional dependence[2] of the form

$$\mathcal{J}_o/\mathcal{J}_{eff} = \begin{cases} a - b\,\ell^2, & \text{for } \ell^2 \le \frac{a-c}{b} \\ c, & \text{for } \ell^2 \ge \frac{a-c}{b} \end{cases} \qquad (4)$$

Here, we have used the rigid sphere moments of inertia (corresponding to the radius R = 1.225* $A^{1/3}$ fm) to obtain the dimensionless numbers $\mathcal{J}_o/\mathcal{J}_{eff}$. For simplicity, the nuclear temperature was calculated from the simple relation T = 7.7 MeV E^*/A, which neglects the spin dependence of the nuclear temperature. The resulting fits are excellent. The best - fit values of $\mathcal{J}_o/\mathcal{J}_{eff}$ as a function of ℓ^2 are shown by the dashed lines in Figure 2. Also included in the Figure are the results of a similar analysis[2] for the reaction ^{32}S+^{208}Pb. The extracted values of $\mathcal{J}_o/\mathcal{J}_{eff}$ are in clear disagreement with the saddle point shapes of the rotating liquid drop model which are shown by the solid curves. For all four cases

investigated, the effective moments of inertia reach asymptotic values $\mathcal{J}_o/\mathcal{J}_{eff} \sim 0.6$ at high angular momenta, corresponding to transition states of rather considerable deformations. At these large angular momenta the fission barriers are expected to vanish, and the reaction is expected to proceed via fast fission[4]. Our observations are in qualitative agreement with recent TDHF calculations performed for heavier systems which indicate that fast fission reactions proceed via rather deformed configurations[5] of the composite system. If, on the contrary, more compact configurations are reached for these reactions our results might indicate that fission fragment angular distributions are not sensitive to these compact configurations because of considerable rearrangement of the angular momentum projections prior to scission.

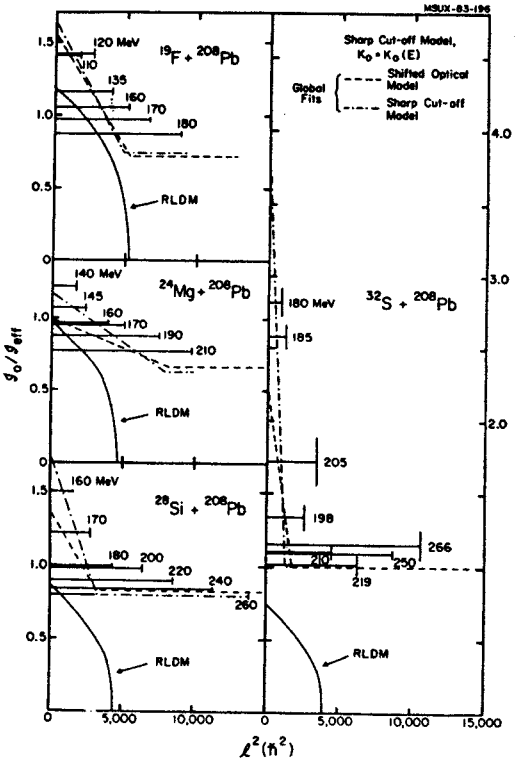

Fig. 2. Angular momemtum dependence of $\mathcal{J}_o/\mathcal{J}_{eff}$ extracted from the analysis of the angular distributions. The dashed and dot - dashed lines are the results of the global fits with the parameterization of eq. 4, using eq. 3 and the sharp cut-off approximation, respectively, for the partial wave fusion probabilities. The solid bars correspond to fits with a constant value for K_o at each energy; for these fits the estimated errors are indicated by the vertical bars and the lengths of the horizontal bars correspond to the range of angular momenta contributing to the fission cross sections. The solid lines show the effective moments of inertia predicted by the rotating liquid drop model.

At energies close to the fusion barrier, rather broad distributions of the partial wave fusion probabilities are obtained from the prescription of eq. 3. It is appropriate to present an analysis of the angular distributions in terms of the more conventional sharp cut-off model for the partial wave fusion cross sections. The two assumptions are then expected to bracket the "true" distribution of the partial wave capture cross sections. Fits of comparable quality as the ones shown in Figure 1 are obtained with the sharp cut-off approximation if one adopts the simple parameterisation of eq. 4 or, alternatively, if one assumes a constant value of $\mathcal{J}/\mathcal{J}_{eff}$ for each energy. The resulting best - fit parameters are shown in Figure 2 by the dot - dashed lines and the solid bars, respectively. Clearly, the discrepancies with the saddle point shapes of the rotating liquid drop model become worse if the sharp cut-off approximation is used.

+ On leave from University of Nantes, Nantes, France.
++ On leave from Physics Department, Sichuan University, Chengdu, Sichuan, PRC.
* Chemistry Division, Argonne National Laboratory, Argonne, IL 60439.
** Nuclear Chemistry Division, Lawrence Livermore National Laboratory, Livermore, CA 94558.

1. R. Vandenbosch and J.R. Huizenga, Nuclear Fisson, Academic Press, New York (1973)
2. M.B. Tsang, D. Ardouin, C.K. Gelbke, W.G. Lynch, Z.R. Xu, B.B. Back, R. Betts, S. Saini, P.A. Baisden, and M.A. McMahan Phy. Rev. C28 (1983) 747.
3. B.B. Back, H.-G. Clerc, R.R. Betts, B.G. Glagola, and B.D. Wilkins, Phys. Rev. Lett. 46 (1981) 1068
4. B. Boderie, M. Berlanger, D. Gardes, F. Hanappe, L. Nowicki, J. Peter, B. Tamin, S. Agarwal, J. Girard, C. Gregoire, J. Matuszek, and C. Ngo, Z. Phys. A299 (1981) 263. B. Boderie, M. Berlanger, D. Gardes, F. Hanappe, L. Nowicki, J. Peter, B. Tamin, S. Agarwal, J. Girard, C. Gregoire, J. Matuszek, and C. Ngo, Z. Phys. A299 (1981) 263
5. H. Stocker, R.Y. Cusson, H.J. Lustig, A. Gobbi, J. Hahn, J.A. Maruhn, and W. Greeiner, Z. Phys. A306 (1982) 235

ANGULAR DISTRIBUTION OF SEQUENTIAL FISSION FRAGMENTS FOR THE REACTION OF 32-S WITH 238-U

D.J. Morrissey, G. Guarino+, G.J. Wozniak+, L.G. Sobotka+, R.J. McDonald+, and L.G. Moretto+

We have taken data on the angular distributions of sequential fission fragments from the reaction of 238 MeV 32-S with 238-U. This is the third measurement in a series of three refs.1,2 of the variation of the alignment of the spin of reaction products with mass asymmetry in deep inelastic reactions. Previous mesurements have used 20-Ne and 40-Ar beams and have shown that the angular distributions of fission fragments depend very strongly on the mass asymmetry of the reaction system.[1,2]

The data were taken at the LBL 88 inch Cyclotron. The 238 MeV 32-S beam irradiated a thin UF_4 deposit on an Al backing. Projectile-like fragments were detected in a gas telescope fixed near the classical grazing angle (69 degrees). The energy and the nuclear charge of the projectile-like fragments were determined by the telescope. Coincident fission fragments were detected in a set of 10 Si surface barrier detectors mounted both in and out of the plane defined by the beam and the scattered projectile-like fragments. Fission fragments were uniquely identified in two dimensional maps of energy and time of flight. The only other reaction channels that were visible were fusion-fission and sequential alpha emission. The fission fragment detectors at forward angles were only 100 microns thick in order to enhance the separation between alpha particles and fission fragments. After passing through the identifying gates the valid coincidences were converted into the calculated rest frame of the target-like fragment on an event by event basis. The angular distributions shown in figure 1 represent some of the results of these transformations. Similar results are available for the out of plane angular distributions.

Preliminary analysis of the in-plane angular distributions show an anisotropy whose magnitude lies inbetween those already established for 40-Ar and 20-Ne induced reactions. This result is, of course, expected but at the same time intriguing. The out-of-plane angular distributions are rather

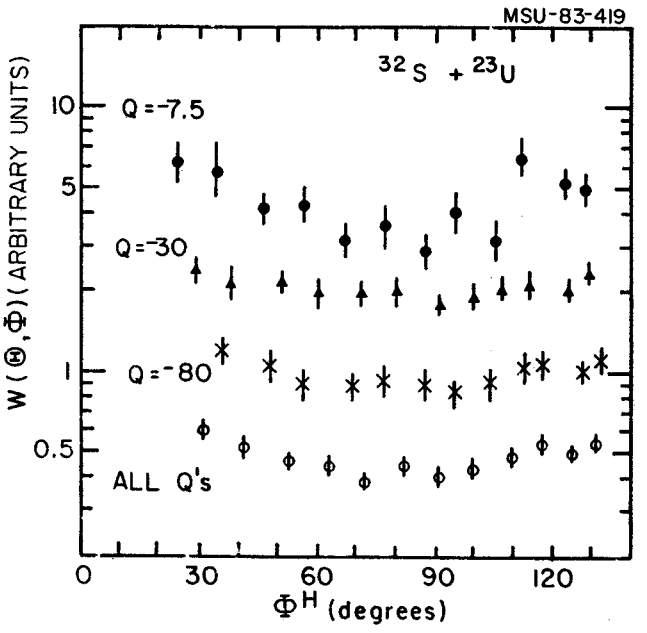

Fig. 1. The in-plane sequential fission angular distributions from the reaction are shown. The top three data sets were generated by gating on the Q-value of the reaction. The angular distribution for the integral over Q-value is shown at the bottom. [MSU-83-419]

flat indicating that the fissioning nucleus has a low spin. The reaction was performed at a low bombarding energy and the deep-inelastic fragments could pick up only rather low spins. The low bombarding energy also limits the range of Q-value over which we can follow the evolution of the spin alignment. However, the fact that the in-plane anisotropy is rather pronounced indicates that the low values of spin are constrained to lie in a plane approximately along the line connecting the centers of the two nuclei at contact. Such a constraint is predicted by statistical equilibrium of the degrees of freedom of two tangent spheres. But the fact that our results show equilibrium for an energy loss of only 7.5 MeV is quite surprising. The results will have to be checked by a complete analysis of the data. During this analysis we will extract quantitative estimates of the spin of the fissioning nuclei and the average orientation of their spin.

+ Permanent address: Lawrence Berkeley Lab, Berkeley, CA.

1. D.J. Morrissey et al., Nucl. Phys. A389,(1982)120.
2. D.J.Morrissey et al., No. 027, this report.

SPIN ALIGNMENT IN THE REACTION OF 40-Ar WITH 197-Au AND 238-U

D.J. Morrissey, G.J. Wozniak[+], L.G. Sobotka[+], A.J. Pacheco[++], R.J. McDonald[+], and L.G. Moretto[+]

We have completed the analysis of the angular distributions of sequential fission fragments from the reaction of 340 MeV 40-Ar with 197-Au and 238-U. Such measurements provide the best probe of the magnitude and orientation of the spin vector of deep inelastic reation products (that can be induced to fission.) This is the second measurement in a series of three /refs.1,2/ of the variation of the alignment of the spin of reaction products with mass asymmetry in deep-inelastic reactions. In our earlier study of 20-Ne induced sequential fission we observed a large anisotropy in the in-plane angular distribution of fission fragments. Any anisotropy indicates a preferred orientation of the spin of the fissioning nucleus. However, the data was concentrated in a very narrow range of exit channel masses. In the present work 40-Ar projectiles were used in order to have a broad range of exit channel masses.

The data were taken at the LBL Super HILAC and analyzed at MSU. Projectile-like fragments were detected in a gas ionizaton telescope which was able to resolve nuclear charges up to Z=36. Coincident fission fragments were detected as a function of angle in an array of 10 surface barrier detectors and cleanly separated from other reaction products in a two dimensional map of energy versus time-of-flight. Two targets were used in the study to increase the range of the mass asymmetry of the reaction products.

Contours of the probability of detecting a sequential fission fragment from reactions with gold and uranium are shown in figure 1 as a function of total kinetic energy (TKE) and projectile-like fragment charge (Z3). The probability contours from reactions with gold are fairly different from those with uranium. This was expected because the gold-like reaction products have significantly higher fission barriers than uranium-like reaction products (in order to obtain the fission probabilities the values presented in fig. 1 should be divided by the singles cross section $d^2\sigma/d\Omega dZ$). But more importantly, a broad range of deep-inelastic reaction products with energy losses of about 150 MeV are in coincidence with fission products from both targets.

The in-plane angular distributions of fission fragments from reactions on gold with an average energy loss of 150 MeV are shown in figure 2. The ungated angular distribution shows a clear anisotropy (1.5:1). When the angular distributions are gated on projectile-like product charge, as also shown in fig. 2, a strong

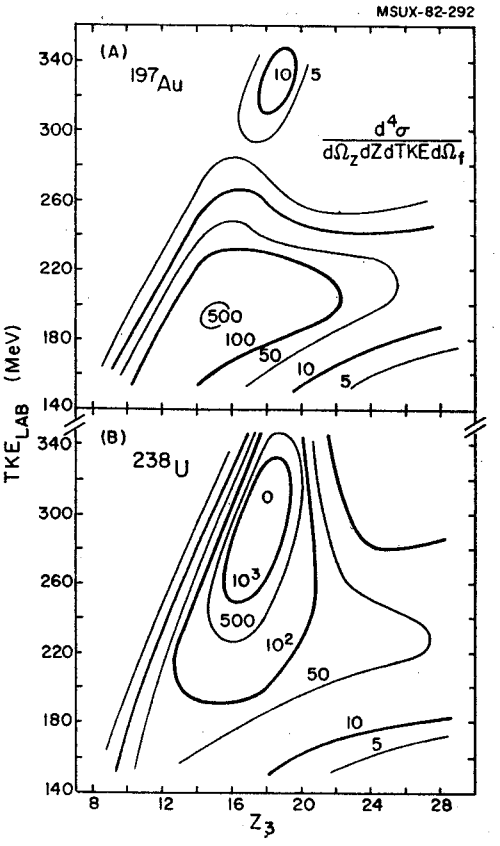

Fig. 1. Contours of the coincidence cross section for detecting a sequential fission fragment are ahown as a function of projectile -like fragment Z and total kinetic energy (TKE) for the two targets used in this study.

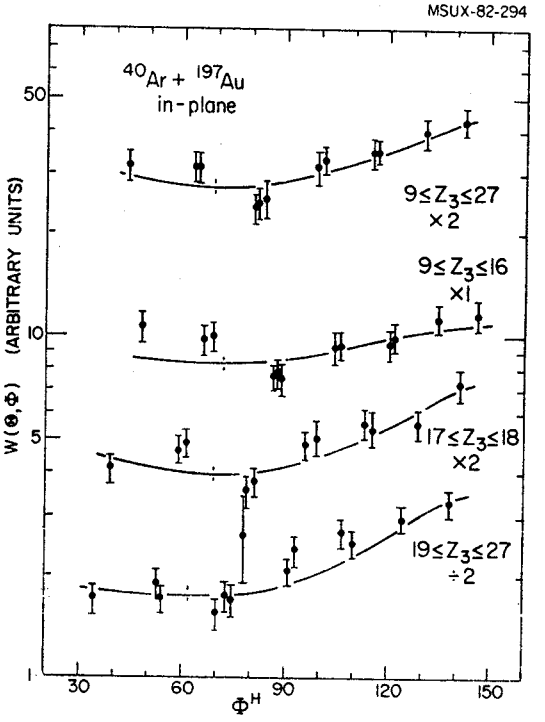

Fig. 2. The in-plane sequential fission angular distributions from the reaction with a gold target are shown. The four data sets were generated by gating on projectile-like fragment charge.

variation of the anisotropy is seen with mass asymmetry of the reaction products. The curves shown in fig. 2 represent an angular distribution function that was fit simultaneously to the in-plane and out-of-plane data for each mass asymmetry bin. Similar results were seen in the uranium data.

We have summarized the results of this and previous work on the anisotropy of sequential fission fragments /ref. 1,3-5/ in figure 3. This figure shows the variation of the in-plane anisotropy parameter:

$$q_3 = (\sigma^2_x - \sigma^2_y) / K^2_{eff}$$

as a function of mass asymmetry of the reaction products. The values of this parameter were extracted from the fitted angular distributions. The energy loses in all the reaction systems are on the order of 150 MeV. Figure 3 shows an overall, or global, decrease of q_3 with mass asymmetry of the reaction. In addition, the anisotropy increases with a similar slope for a

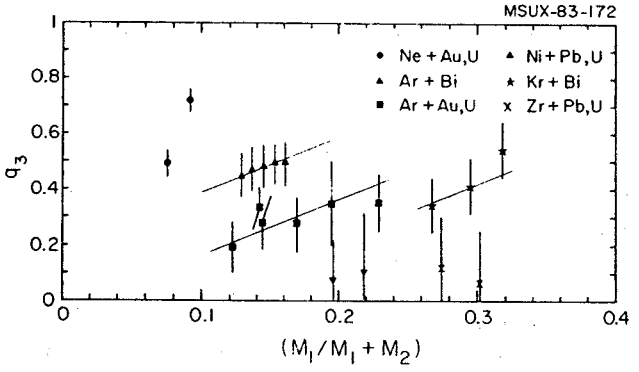

Fig. 3. The calculated in-plane anisotropy parameter, q_3, is shown as a function of mass asymmetry of the fragments in the exit channel of ten different deep inelastic reactions. The global decrease of asymmetry with decreasing mass asymmetry is discussed in the text.

fixed entrance channel. This latter variation is most likely due to changes in eff. This parameter describes the ability of the fission fragment angular distribution to carry information on the spin distribution of the fissioning nucleus. K^2 eff depends on the saddle point shape and certainly varies with the mass of a fissioning nucleus. The global variation is consistant with statistical equilibrium of the rotational degrees of freedom of two rigid spheres in contact. However, the magnitude of the observed in-plane anisotropy is much larger at mass asymmetries between 0.15 and 0.3 than the model predictions. Thus, the control of the spin alignment of the reaction partners is not as simple as that of two rigid spheres. But at the same time the controlling mechanism is not that different.

+ Permanent address: Lawrence Berkeley Lab, Berkeley, CA.

++ Permanent address: Comision Nacional de Energia Atomica, Buenos Aires, Argentina.

1. D.J. Morrissey et al., Nucl. Phys. A389,(1982)120.
2. D.J. Morrissey et al., No. 028, this report
3. P. Dyer et al., Nucl. Phys. A322(1979)205.
4. D.v. Harrach et al., Phys. Rev. Lett. 42(1979)1728.
5. C. LeBrun et al., Phys. Rev. C25,(1982)3212.

MEASUREMENT OF A=1-14 FRAGMENTS AND CLUES TO THE ENTROPY CREATED IN NUCLEAR COLLISIONS

B.V. Jacak, G.D. Westfall, C.K. Gelbke, L.H. Harwood, W.G. Lynch, D.K. Scott, H. Stoecker, M.B. Tsang, and T.J.M. Symons*

Systematic measurements of large nuclear fragments at velocities intermediate between that of the projectile and target have been made. Calculations with a quantum-statistical model of thermal and chemical equilibrium among the various fragments and with a Hauser-Feshbach model of sequential particle emission followed by cooling of the system reproduce the observed relative inclusive production cross sections of fragments with $1 \leq A \leq 14$. These calculations provide a method of extracting the entropy per nucleon of the system. The expansion of the initial reacting system is nearly isentropic [1], thus the entropy extracted from the final fragment distribution reflects the entropy created during the early stages of the reaction.

The measurements were carried out at the Lawrence Berkeley Laboratory Bevalac using ^{40}Ar beams of 42, 92 and 137 MeV/ nucleon. Targets consisted of 80 mg/cm^2 and 200 mg/cm^2 Au. Calcium targets were also used, and the data show features similar to those observed with gold. Heavy fragments were measured with two stacks of silicon detectors, which were calibrated with direct beams of ^{20}Ne. Light particles (p,d,t, ^3He, ^4He, and ^6He) were measured simultaneously with a telescope consisting of two silicon ΔE detectors and a NaI E detector, and calibrated with proton and alpha beams. All telescopes covered an angular range of 30 to 130 degrees in 20 degree steps, and isotope resolution from hydrogen through carbon was achieved.

The energy spectra and angular distributions were fitted using a single moving source model [2]. In the model it is assumed that each fragment is emitted according to a relativistic Boltzmann distribution in the rest frame of the source. This parameterization is useful in isolating the component of inclusive spectra arising from an intermediate velocity source. For $A \leq 6$, particles emitted at lab angles 50° and larger and at energies above evaporation energies were included in the fits. The thickness of the first detectors in the heavy ion telescopes was chosen to preclude measurement of evaporation products. Heavy projectile fragments are peaked far forward of 30°, so all of the measured data for fragments with A>6 were used in the determination of the moving source parameters. The extracted source temperature for each fragment is shown as a function of the fragment mass in Fig. 1. The

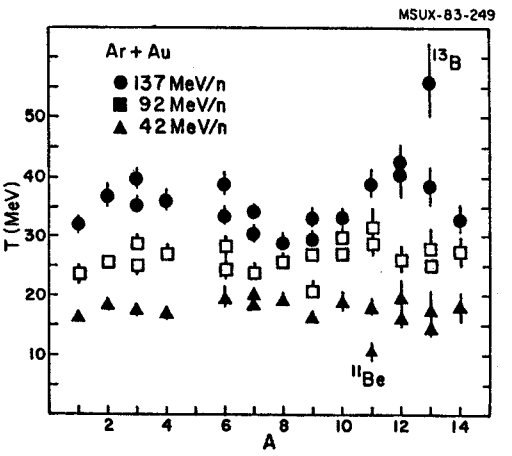

Fig. 1. Temperatures obtained from fitting the fragment energy spectra with a single moving source, as a function of the fragment mass for three bombarding energies. Where two points for a single mass are shown, two fragments of that mass were observed.

temperatures for various fragments at one bombarding energy are very similar, suggesting that the observed fragments originate from a thermal source, and that the same type of source gives rise to the heavy and the light fragments.

The single source fits were integrated to yield the production cross section for each fragment. Fig 2a shows these cross sections as a function of fragment mass for the three bombarding energies. The error bars reflect the error induced by extrapolation of the data to unmeasured angles and energies. The solid histograms show the results of a quantum statistical calculation [3,4]. The calculation is performed for a given N/Z, breakup density and entropy/nucleon (S/A) and treats fermions and bosons in thermal and chemical equilibrium. The calculated relative cross sections as a function of mass for a given S/A are nearly independent of the breakup density in the range of 0.3-0.7 times normal nuclear matter density, ρ_o. The results shown in Fig. 2a are for $\rho = 0.5\rho_o$. The dashed histograms result from a Hauser-Feshbach model of statistical particle emission [5]. Particles are assumed to be emitted from an excited nucleus at constant density and the temperature, charge and mass evolution of the system is followed. The entropy is extracted by treating the system as a Fermi gas, and depends only slightly on the density over the range of 0.5 to 1.5 times normal nuclear matter density. The histograms in Fig. 2a are from calculations at $\rho = \rho_o$.

The results of both calculations follow the trend of the data. Neither model incorporates assumptions about the dynamics of the reaction, but the models treat the breakup of the system very differently. The entropy/nucleon deduced with these models is consistent to within S/A=0.2

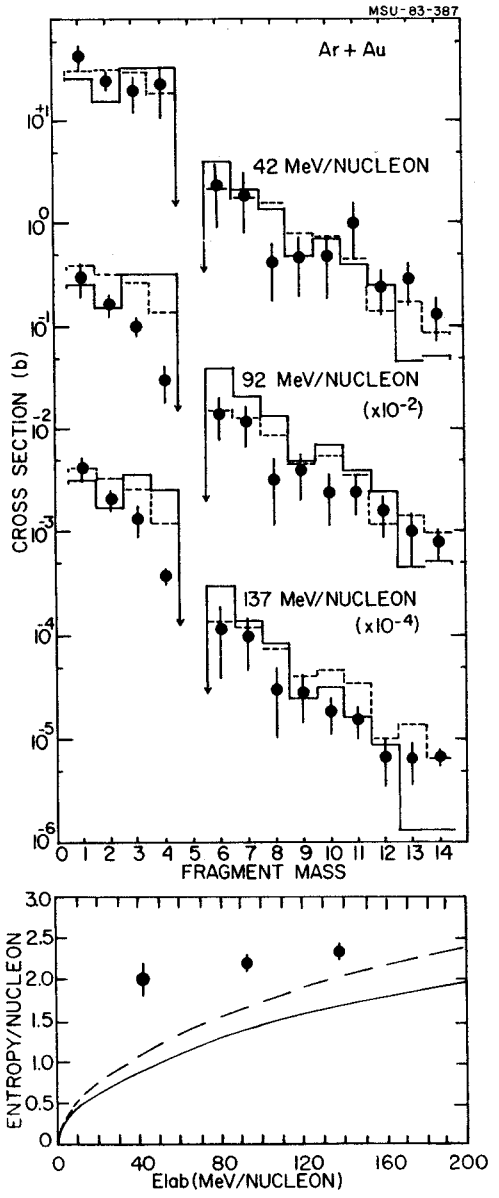

Fig. 2. a) Relative productions cross sections of fragments with A=1-14 at 42, 92 and 137 MeV/nucleon. The solid histograms are the results of a quantum statistical model and the dashed histograms the result of Hauser-Feshbach calculations.

b) Entropy extracted from the model fits to the fragment distributions, as a function of bombarding energy. The solid line is the entropy expected from a perfect fluid dynamical calculation, and the dashed line is the prediction for a viscous fluid [6].

and the extracted values of S/A = 2.0+/-0.2, 2.25 +/- 0.25 and 2.35 +/- 0.2 for 42, 92 and 137 MeV/nucleon Ar + Au, respectively, are shown in Fig 2b. The solid line shows the entropy/nucleon expected for central collisions in a hydrodynamic calculation and the dashed line for a viscous fluid [6]. The entropies extracted from these data are closer to expectations from conventional models than the entropies deduced via a simplified description based on deuteron to proton ratios [7], which are typically S/A=4-6 in this energy regime.

* Lawrence Berkeley Laboratory, Berkeley, Calif.

1. G. Bertsch and J. Cugnon, Phys.Rev.C24 (1981)2514.
2. G.D. Westfall, B.V. Jacak, N. Anantaraman, M.W. Curtin, G.M. Crawley, C.K. Gelbke, B. Hasselquist, W.G. Lynch, D.K. Scott, M.B. Tsang, M.J. Murphy, T.J.M. Symons, R. Legrain T.J Majors, Phys.Lett 116B (1982) 118.
3. J. Gosset, J.I. Kapusta and G.D. Westfall, Phys.Rev.C18 (1978) 844.
4. H. Stocker, G. Buchwald, G. Graebner, P.Subramanian, J.A. Maruhn, W. Greiner, B.V. Jacak and G.D. Westfall, Nucl.Phys. A400 (1983) 63c.
5. W.A. Friedman and W.G. Lynch, Phys.Rev.C28 (1983). 16.
6. H. Stocker, Lawrence Berkeley Laboratory Report 12302.
7. P. Siemens and J. Kapusta, Phys.Rev.Lett. 43 (1979) 1486.

NEUTRON AND GAMMA EMISSION FROM $^{156}Er^*$ after ^{64}Ni + ^{92}Zr and ^{12}C + ^{144}Sm REACTIONS

W. Kühn*, P. Chowdhury**, R.V.F. Janssens***, T.L. Khoo***, G. Rossner***, F. Haas+, J. Kasagi++, and R.M. Ronningen

In last year's Annual Report we showed preliminary results from our study of the ^{64}Ni + ^{92}Zr reaction at 233 MeV (corrected for energy loss in the target). Neutron and gamma spectra were obtained in coincidence with total (sum) gamma ray energy. We obtained neutron spectra for different slices of the sum energy spectrum and deduced the "temperature" of each spectrum from a fit to its exponential tail. The entry line spins for each sum energy slice were determined from the γ-ray multiplicities. Figure 1 shows the neutron spectra, their temperatures and corresponding entry line spins.

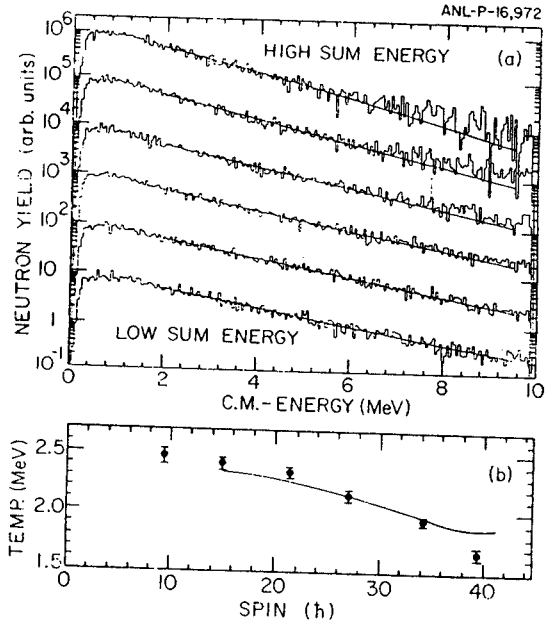

Fig. 1

Fig. 1. (a) Neutron spectra, measured at 0°, for six consecutive gamma ray sum energy slices. The straight lines represent fits with an exponential function in the energy interval spanned by the lines. Deviations from the exponential shape at high sum energy are due to contamination from isomeric gamma rays.
(b) "Temperatures", derive from the fits in Fig. 1a, as a function of mean entry line spin corresponding to the different sum slices. The solid line represents results from similar fits to neutron spectra obtained in CASCADE calculations, using the elevated (dashed) yrast line and a level density parameter a = A/15.

The neutron multiplicity distribution was deduced from the yields of $^{155,154,153,152}Er$ observed in the high resolution Ge spectra. The distribution is shown in Fig. 2 along with predictions by the statistical model code CASCADE, modified to include enhancement of collective E2 transitions parallel to the yrast line and E1 deexcitation through the giant dipole resonance. These predictions (solid bars) underestimate the ratio of 2n to 3n emission by a factor of twenty. No modification of the model parameters within reasonable limits could significantly improve this. The suppression of the third neutron suggests that the available free energy for neutron emission (above the compound nucleus yrast line) is about 10 MeV smaller than expected. One way to raise the yrast line to form a "deformation trap"- a superdeformed shape at high spin and energy which "lives" for a time comparable to neutron emission times. Introducing an yrast line corresponding to a superdeformed shape[1] results in the dashed bars in Fig. 2.

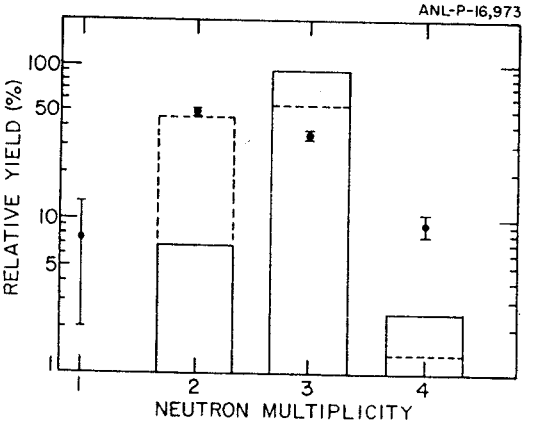

Fig. 2

Fig. 2. Comparison of experimental (circles) neutron multiplicity distribution with those from statistical model calculations using the normal (solid bars) and elevated (dashed bars) yrast lines.

This past year we have undertaken a study of the neutron multiplicity distribution as a function of bombarding energy and entrance channel using ^{64}Ni + ^{92}Zr (225, 235, 245, 255, 270, and 75 MeV) using beams from the Argonne National Laboratory Superconducting Linac. Neutron spectra were obtained in the 225 MeV ^{64}Ni-induced reaction and in the 68 MeV ^{12}C-induced reaction. The latter produces $^{156}Er^*$ in an excitation energy and spin state most nearly equivalent to $^{156}Er^*$ produced by the 233 MeV Ni-induced reaction. The mass asymmetry of different entrance channels may lead to different initial deformations of the fused systems.

* Present address: II. Physikalisches Institut, Universitat Giessen, W. Germany.
** Present address: Niels-Bohr Institute, Copenhagen, Denmark.
*** Argonne National Laboratory.
+ Permanent address: C.R.N. Strasbourg, France.
++ Present address: Tokyo Institute of Technology, Tokyo, Japan.

1. S. Åberg, Phys. Scripta 25, 23(1982).

PION PRODUCTION FROM $^{139}La+^{139}La$ AT E/A=245 MeV

K. Beard*, W. Benenson*, B. Sherrill*,
J. VanderPlicht*, L. Schroeder**, H. Pugh**,
J. Miller**, P. Kirk***,
G. Krebs***, J.-F. Gilot***,
J. Harris+, G. Roche++ and J. Vincente++

Investigation of nucleus-nucleus collisions have been extended to much heavier systems by the recent Bevalac upgrade. This enables further searches for collective phenomena, for example a new phase of pionic instability related to pion condensation, predicted by M. Gyulassy[1] for subthreshold pion production at 90 deg c.m.. Earlier searches for the same phenomenon by Nagamiya[2] using Ne+NaF found no sign of pion condensation. Extension of the search from mass 20 to mass 139 increases the possibility of observing the condensation as an enhancement of the pion spectrum predicted to be a bump on the exponentially decreasing cross section at a pion c.m. energy of 280 MeV.

This experiment used one arm of the TASS (Two Arm Spectrometer System) at the Bevalac at LBL. The targets were in vacuum with an exit window immediately downstream. The pions travelled through air, a hodoscope, a large dipole magnet gap, two hodoscopes, two position sensitive wire chambers, a scintillator, and a Cherenkov counter. An ion chamber downstream of the target measured the beam current. Symmetric targets and beams were used so that the center of mass would be well defined and independent of intermediate size.

Calibration data was taken with 800 MeV/A Ne on NaF so as to be able to compare to previous pion data. The preliminary results of the experiment, which are shown in Fig. 1, indicate a straight exponential decrease with pion energy in the center of mass frame, as would be expected for a thermal source. The slope of the 90 deg spectrum gives a temperature of 37 MeV, which is about what one would expect for this beam energy. In addition one shift was devoted to a measurement at 50 deg c.m. This spectrum, which does not extend out nearly as far in pion kinetic energy as the 90 deg data do, gives a similar slope but with much poorer statistics. A further experiment to verify this result and to extend this first experiment on subthreshold pion production with really heavy ions to more forward angles is planned for the spring of 1984.

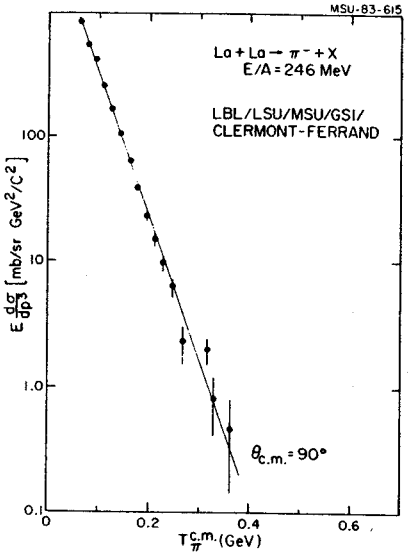

Fig. 1. Preliminary results for pion production with La +La at 90 deg and E/A= 245 MeV.

1. M. Gyulassy, "Current Topics in Relativistic Nuclear Collisions", Nucl. Phys. A354, 395 (1981).
2. S. Nagamiya, et al., "Production of Negative Pions with 183/nucleon Beams" Phys. Lett. 48, 1780 (1982).

* National Superconducting Cyclotron Laboratory, Michigan State University, E. Lansing, MI 48824.
** Lawrence Berkeley Laboratory, Berkeley, CA.
*** LSU
+ LBL/GSI
++ Clermont-Ferrand